COMMISSARIAT A L'ENERGIE ATOMIQUE

CENTRE D'ETUDES NUCLEAIRES DE SACLAY
Service de Documentation
F91191 GIF SUR YVETTE CEDEX

CEA-CONF --10104

L5

I.C.F. PROGRAM AT CEL-V

ANDRE M.- COUTANT J.- DAUTRAY R.- DECOSTER A.- DECROISETTE M.
DUBORGEL B.- OUVRY J.- OVADIA J.- WATTEAU J.P.
CEA Centre d'Etudes de Limeil, 94 - Villeneuve-Saint-Georges (FR)

Communication présentée à : 20. European Conference on Laser-Matter Interaction

Schliersee (DE)
22-26 Jan 1990

I.C.F. PROGRAM AT CEL-V

M. André, J. Coutant, R. Dautray, A. Decoster, M. Decroisette, B. Duborgel, J. Ouvry, J. Ovadia, J.P. Watteau

Commissariat à l'Energie Atomique,
Centre d'Etudes de Limeil-Valenton
94195 Villeneuve-Saint-Georges, France

ABSTRACT

The principal objective of the CEL-V laser program is to realize high performances ablative implosions. The indirect drive approach has been chosen to reach the high degree of uniformity required. In relation to this objective, the radiation transfer and the development of hydrodynamics instabilities are widely studied. Besides, efforts have been developed in the field of diagnostics, and of laser technology with optical smoothing and high damage level coatings studies.

1. IMPLOSION PHYSICS

1.1. Radiation driven implosions

High yield implosions involved in Inertial Fusion Confinement require a low preheat, a high degree of drive energy uniformity, and a minimum development of hydrodynamics instabilities.

A drive asymmetry of the order of 1 % seems permissible to reach the high convergence ratios (30-40) needed to achieve ignition [1]. In the direct drive approach, several optical smoothing techniques have been proposed to improve the on-target irradiance uniformity : induced spatial incoherence (ISI) [2], echelon free ISI [3], distributed phase plates [4], smoothing by spectral dispersion [5], or optical fiber oscillator [6]. Even with such devices, a high number of overlapping laser beams appear necessary : with the 24 beams equipped with DPP of the OMEGA laser system, Rochester reached a non-uniformity level of ≈ 10 % (RMS) [7]. In the indirect approach, the visible or UV laser radiation is converted into soft X rays used to implode a fuel capsule inside a hohlraum target. Compared to the previous configuration, the drive uniformity is greatly enhanced ; LLNL with the 10 beams NOVA laser got a uniformity better than 3 % [8].

The direct laser irradiation scheme (DD) is the most efficient in terms of energy transfer into the capsule. However, lesser constraints on beams number and quality, and a better drive isotropy may give a substantial advantage to the indirect scheme (ID).

An irradiation defect $\Delta\phi$ will result, after the acceleration stage, in a velocity defect Δv of the pusher such that $\Delta V/V = k.\ \phi/\phi$, where k is the power index of ϕ in the relation between irradiance, ablation pressure and ablated mass ratio :

$$Pa/\dot{m} \propto \phi^k$$

Assuming a nearly constant implosion velocity, and bringing in that the energy to invest is inversely proportional to the square of the final fuel density, we get a rough estimate of the ratio between the DD and ID laser energies required to get the ignition with a given maximum defect of core sphericity and for the same relative initial irradiation defect $\Delta\phi/\phi$:

$$\frac{E_{DD}}{E_{ID}} = \frac{\eta_{I.D}}{\eta_{D.D}} \left(\frac{k_{DD}}{k_{ID}}\right)^6$$

where η is the efficiency of laser energy transfer to the fuel. With $k_{DD} = 0,33$ [9], and $k_{ID} \approx 0,17$ [10,11], assuming $\eta_{ID}/\eta_{DD} = 0,1$, we get a laser energy for indirect drive $\approx$ 6 times lesser than for direct drive. Obviously, preheat and hydrodynamic instabilities should be taken in account for a more accurate evaluation.

Radiation driven implosion is the approach hold and studied by CEL-V. In order to attain this objective, radiation transfer has been studied for a long time [12]. The level of implosion symmetry in different kinds of hohlraum targets has been estimated using glass capsules. Experiments have been performed either with Octal or with Phebus. It was verified that the sphericity could be improved by a proper choice of geometry, even with two beams only.

The figure 1 shows time integrated X-ray pictures of the core emission for different situations, showing the progression towards a nearly 1D implosion. The factor b/a stands for the ellipticity of the core ; the last recording in the series of 2 beams implosions has been partly occulted by the hohlraum structure.

1.2. Radiation transfer

The physics of radiation transfer has been studied for a long time, in so far as necessary studies to succeed in the previous goal. Numerous series of experiments have been performed using the different laser facilities at the CEL-V : P 102, OCTAL, and PHEBUS to analyse the fundamental properties of X-ray conversion - i.e : efficiency, lobe, spectra - as a function of target characteristics and irradiation conditions.

In 1982, we presented in the same conference results obtained on thick planar targets, and proposed an analytical expression giving the X-ray conversion rates, useful to get easily their evolution versus the interaction parameters [13]. The greater part of the X rays emission is located below 1 keV ; the efficiency increases with the target atomic number and the laser frequency. In gold, up to 5 % of the X-ray energy are

INDIRECT DRIVE IMPLOSION EXPERIMENTS AT CELV

The implosion symmetry is controlled by varying hohlraum geometry

. Core X-ray emission is observed :

for two Laser beams , versus hohlraum geometry

for eight Laser beams

b/a = 1.1

1 DIM

ΔR / R = 20 %

Fig. 1 Time-integrated X-ray pictures of core emission from X-ray driven implosions

carried in M lines, between 2 and 3 keV, and in Copper 10 % are carried in L lines, with a spectral peak between 1.1 and 1.5 keV. An X-ray conversion efficiency up to 60 % has been measured with Phebus for irradiances $\simeq 10^{14}$ W cm^{-2} at λ = 0.35 µm in 0,7 ns pulse duration (fig. 2). The front side emission lobe is intermediate between isotropic and Lambert's law.

In 1987 [14], complementary studies have been performed in thin targets ; the rear side emission appeared to present a maximum in efficiency (20 % of the laser energy) for defined couples : target thickness-laser irradiance, with a rise-time increasing versus the target thickness. Experimental results can be satisfactorily restituted provided a non LTE physics is included in the codes (fig. 3). The evolution in time of the rear side emission is recorded with a broad band spectrometer constitued of a transmission grating (period 5000 A) for spectral dispersion, associated with a soft X-ray streak camera providing a 50 ps mm^{-1} sweep velocity and a time resolution ≈ 30 ps. A typical recording is shown fig. 4a. It has been obtained with a 2 µm thick gold foil irradiated at an irradiance I ≈ 3 10^{13} W cm^2 with a 0,35 µm 0,7 ns laser pulse. The signal represents the intensity of emission in the spectral range 6-7,5 A. It roughly starts in step with the laser pulse. A shoulder is clearly observed over ≈ 400 ps after the leading edge, followed by a well pronounced peak at t ≈ 800 ps. They are respectively identified as the breaking through of the shock and of the radiation wave [15]. The laser irradiance being fixed, it appears that such a situation is very sensitive to the target thickness ; for thin foils, the shock is too short to be detected, while for thicker ones the radiation wave fades before breaking out. Numerical simulations are in a quite good agreement with experimental data (fig. 4b). In same experiments, the hydrodynamical behaviour of the target has been observed using a streaked soft X-ray imaging device composed of a slit for spatial resolution and a streak X-ray camera. The observation was tangential to the target, the spectral range of recording was $h\nu \approx$ 100-300 eV. An experimental result and the corresponding numerical simulations are shown fig. 5. The time delay to get a significative X-ray emission on the rear side ($\Delta t \approx$ 300 ps) is also clearly evidenced.

1.3. Effect of optical smoothing

In relation to this program, the influence of beam optical smoothing on X-ray conversion has been studied. Smoothing was obtained using the techniques of optical fibre [16] allowing to perform experiments at λ = 1.05, 0.53 and 0.35 µm. The laser pulse duration was $\Delta t \approx$ 1.4 ns, and the laser irradiance was varied between a few 10^{12} W cm^{-2} to 9.10^{13} W cm^{-2}. The experimental data concern the emission lobe (fig. 6a) and the conversion efficiency (fig. 6b). No significant increase of X ray conversion was observed, by comparison with previous results [13]. The same observation was mentionned by LLNL and KMSF Inc. [17]. But we found out a greatly enhanced reproducibility of experiments, as shown for example in the small data spreading in fig. 6a. Moreover, we observed at λ = 0.53 µm that the hard X ray emission ($5 < h\nu_{keV} < 20$) is reduced by a

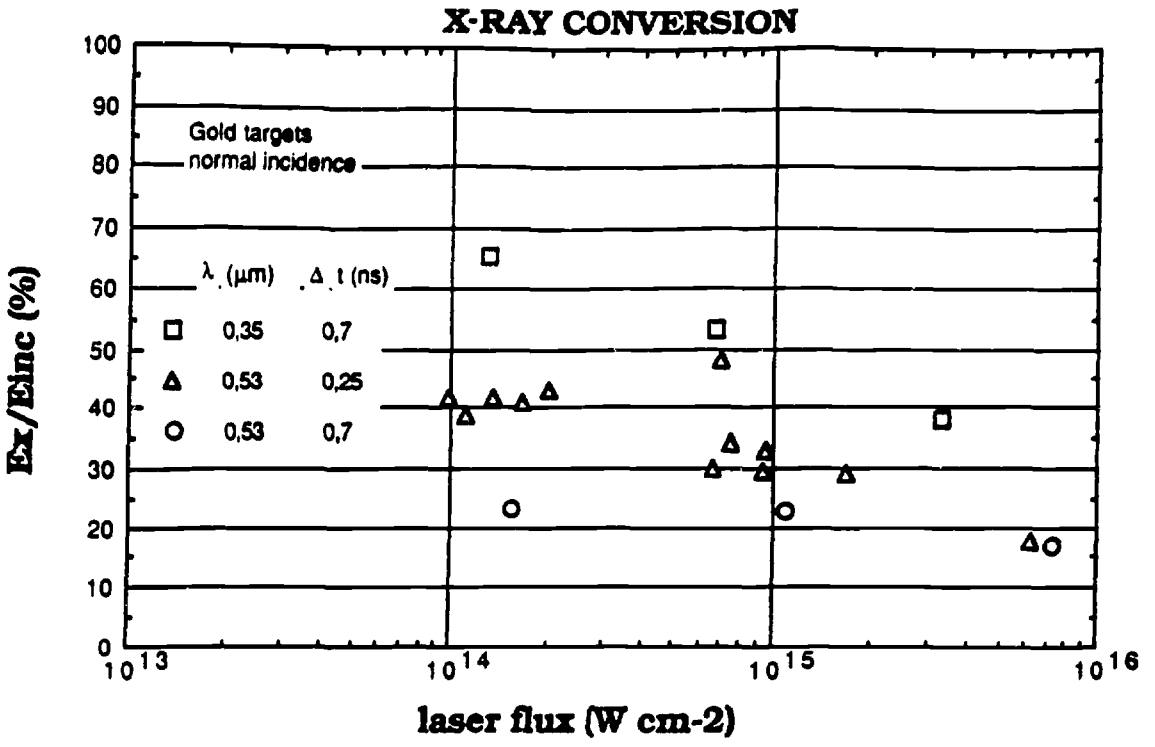

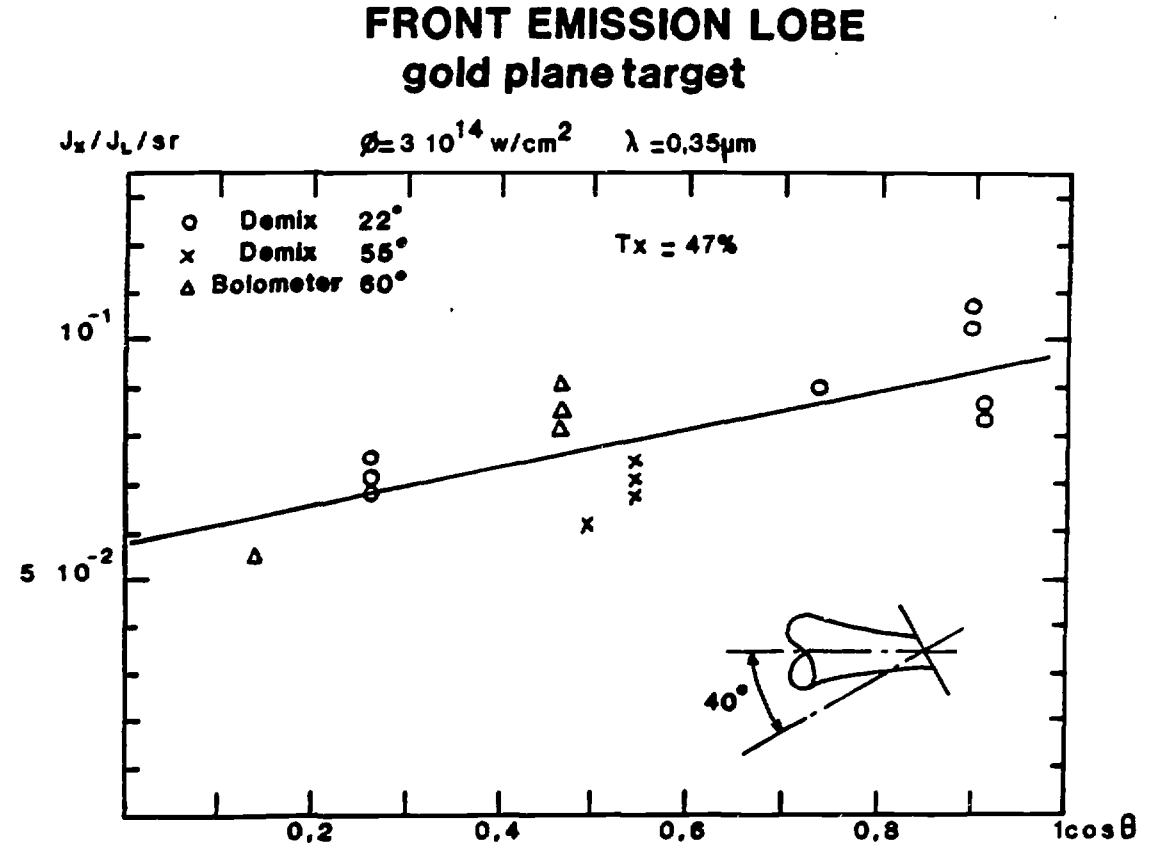

Fig. 2 X-ray conversion efficiency and front emission lobe from planar thick gold targets

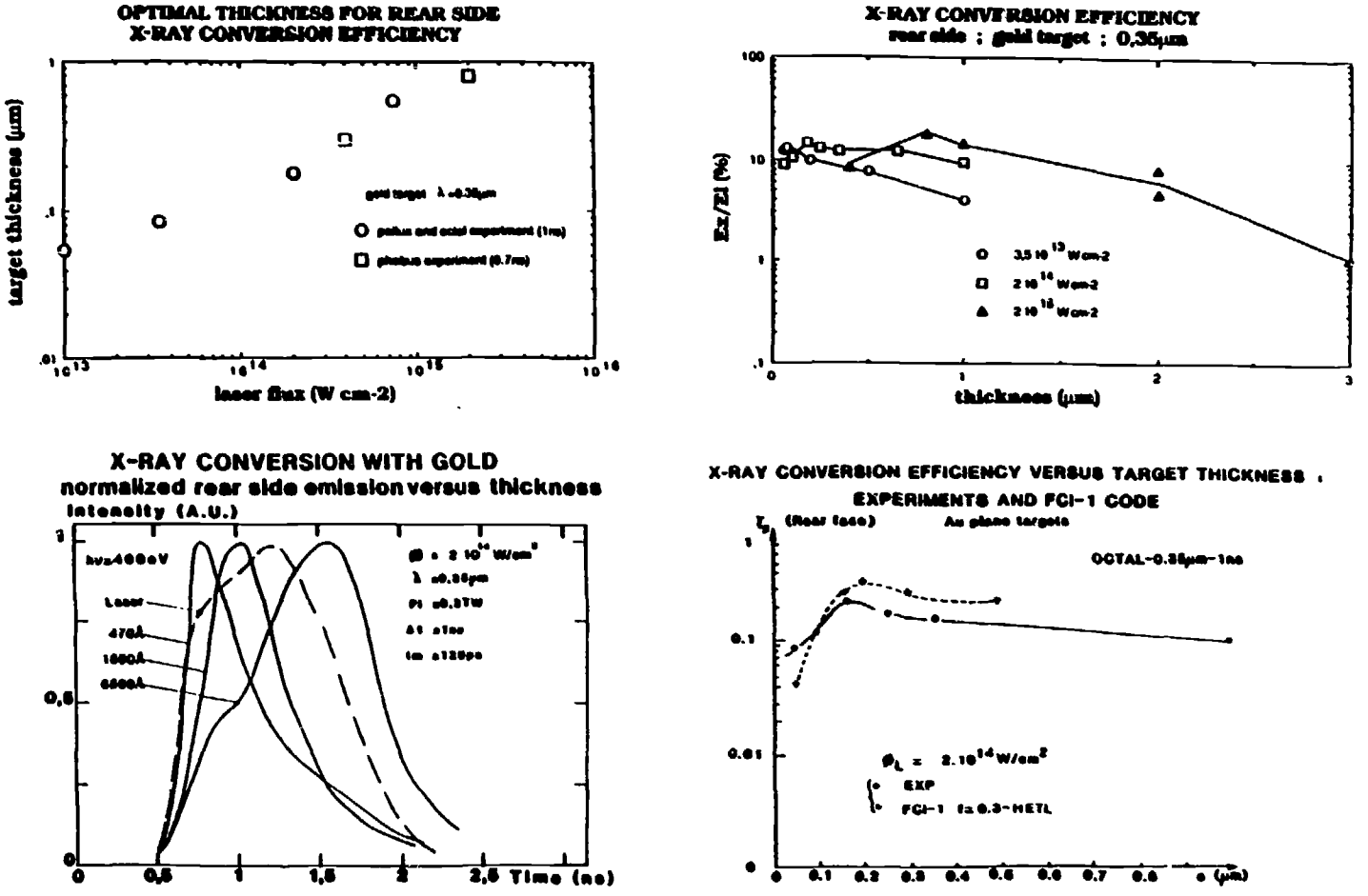

Fig. 3 Main features of rear side X-ray emission from thin gold targets (e < 1 µm)

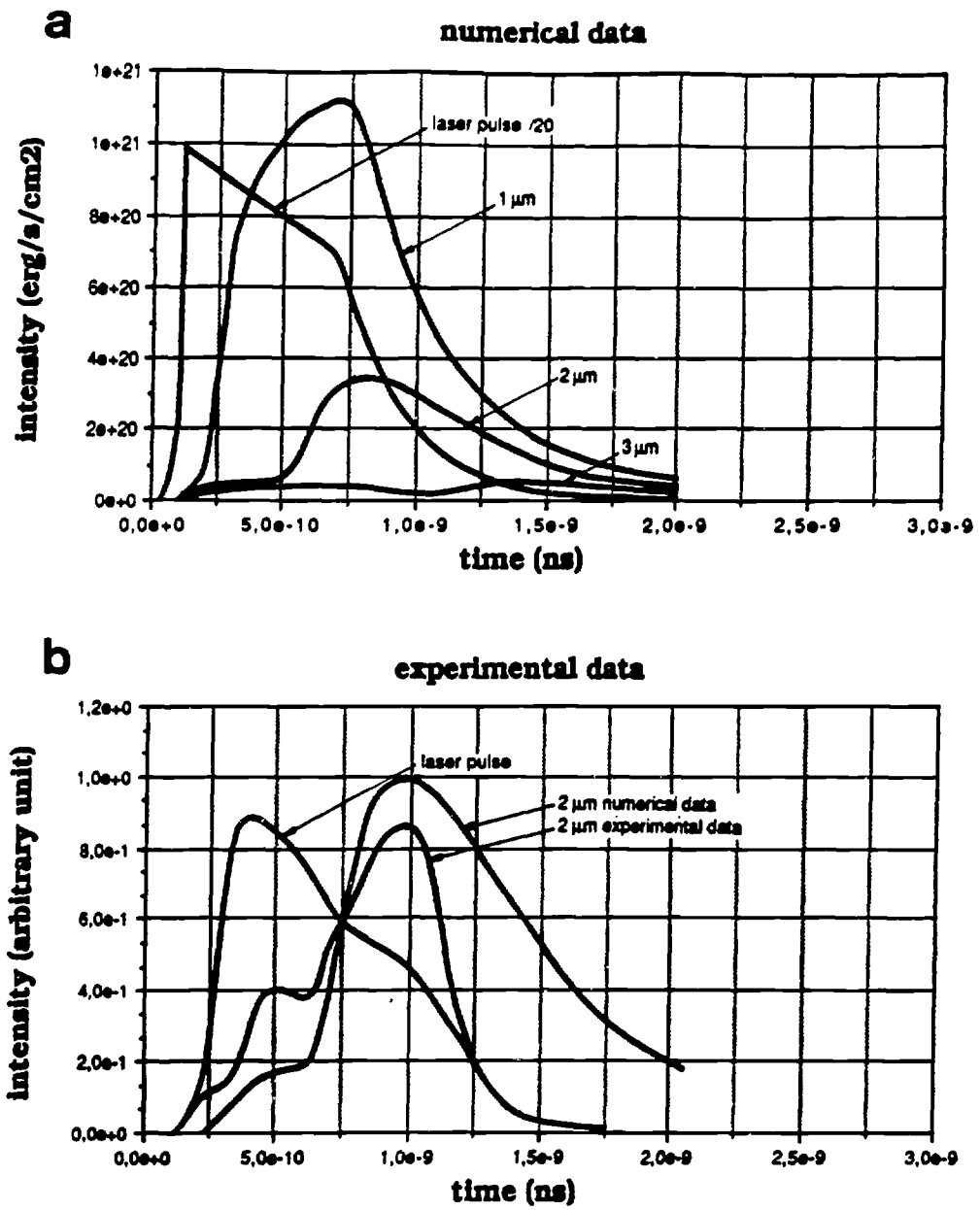

Fig. 4 Compared experimental data and numerical simulation of rear side X-ray emission for planar gold layers (e > 1 µm)

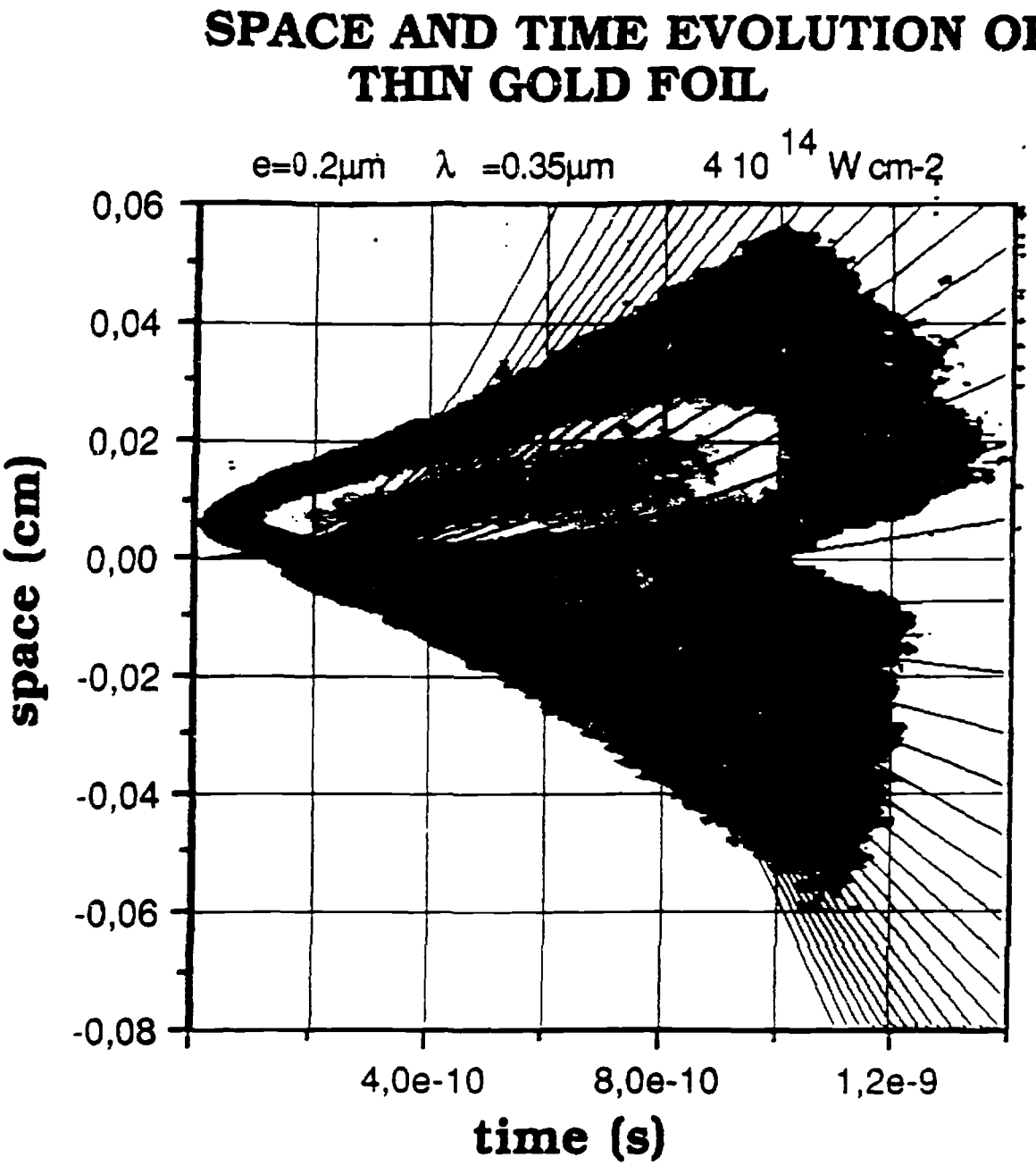

Fig. 5 Hydrodynamical behaviour of a laser irradiated thin gold target. Streaked soft X-ray recording ; superimposed 1D numerical simulation

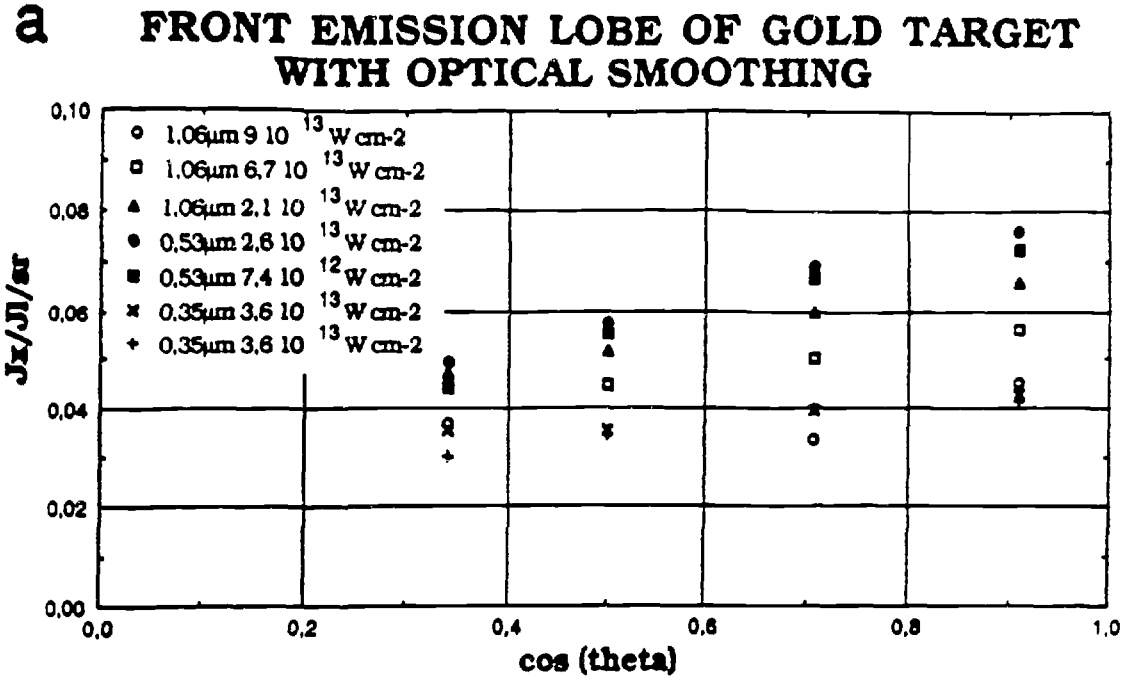

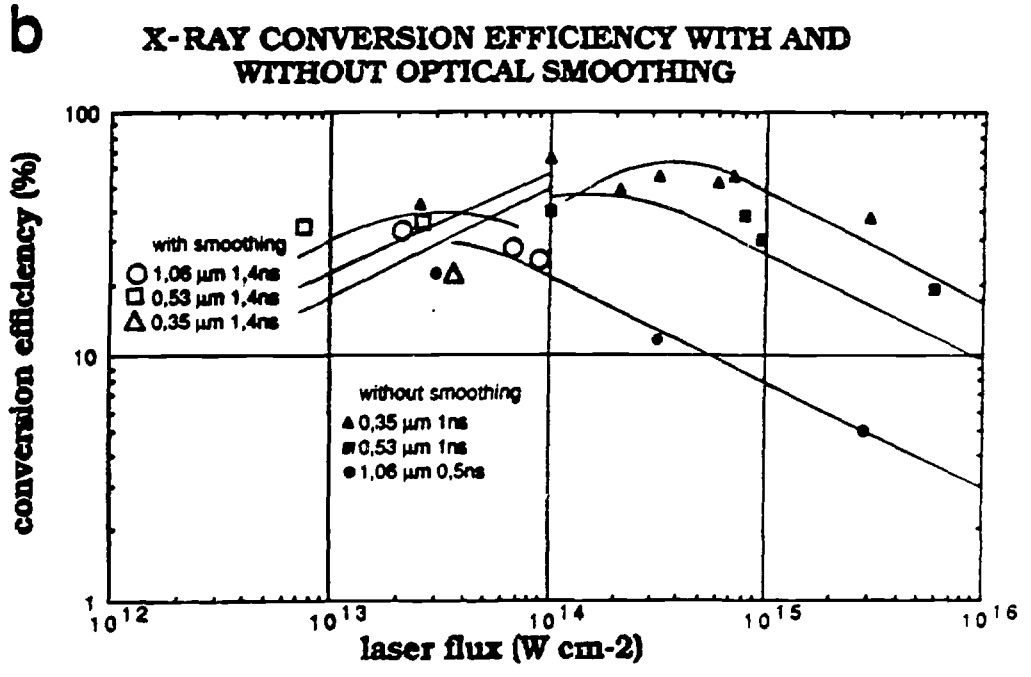

Fig. 6 X-ray emission from gold targets irradiated with a smoothed beam : front emission lobe and conversion efficiency compared with non-smoothed beam results

factor ≈ 10, by comparison with experiments using classical beams (fig. 7). This effect can be attributed to a reduction of Raman instability which, in a classical beam, can be enhanced for several reasons such as hot spots where the laser intensity becomes higher [18].

The effect of optical smoothing on the ablation depth has also been studied in gold planar targets [19]. We observed that at 1,06 µm the ablation depth was unchanged by smoothing the laser, and was 3 times the depth given by the hydrocodes ; that may signify that the process is dominated by filamentation. At 0,53 µm and 0,35 µm, the ablation depth is in agreement with the code, whatever the smoothing method is used (Fig. 8).

1.4. Hydrodynamic instabilities

Hydrodynamic stability remains one of the major question adressed in the field of Inertial Confinement Fusion. Instabilities can occur at the DT-pusher interface during the slowing-down stage, give rise to mixing of the DT with the pusher and lower the implosion performances.

We study the development of the mixing zone in plasma situation using laser-accelerated tri-layer planar targets. In fact instead of "mixing" it would be more rigourous to say "interpenetration" of the fluids because we do not know the real state of the fluids, at least for the experimental point of view.

The experimental setup and the principles used in Limeil have been already published [13] : the target is a foil made of Au/Al/Au ; a probe beam heats the rear gold layer over a small fraction of its thickness (1/3). Once the target is irradiated by the driver beam, the shock and the acceleration can induce Richtmyer-Meshkov and Rayleigh-Taylor instabilities at the rear Al/Au interface. If the mixing is scarcely developed, a spectroscopic observation of the rear of the target will reveal gold emission only ; if the mixing zone is broadly developed aluminium line Heα will be detected.

In the first campaign, the experimental conditions were [13,20] :
- trilayer foils Au(0.3 µm)/Al(2 µm)/Au(0.3 µm)
- the driver-beam features were: 0.35µm, 1ns FWHM and from 1 to 3 10^{13} W/cm²
- the probe-beam features were : 1.06µm, 1ns FWHM, delayed by 1ns with respect to the driver beam and 3.10^{13} W/cm² ; the probe depth measured was 0.1 µm of Au, that is, 1/3 of the total gold thickness.

We gave evidence of some mixing between gold and aluminium for a driver intensity larger than 10^{13} W/cm² ; moreover we compared the Al line emission given by trilayer foils and those ones given by pre-made mixing with a given rate of aluminium atoms : for intensities in the range 2-3 10^{13} W/cm² an agreement is obtained for mixing with 20 % of Al and 80% of Au.

For the second campaign, we brought the following improvements:

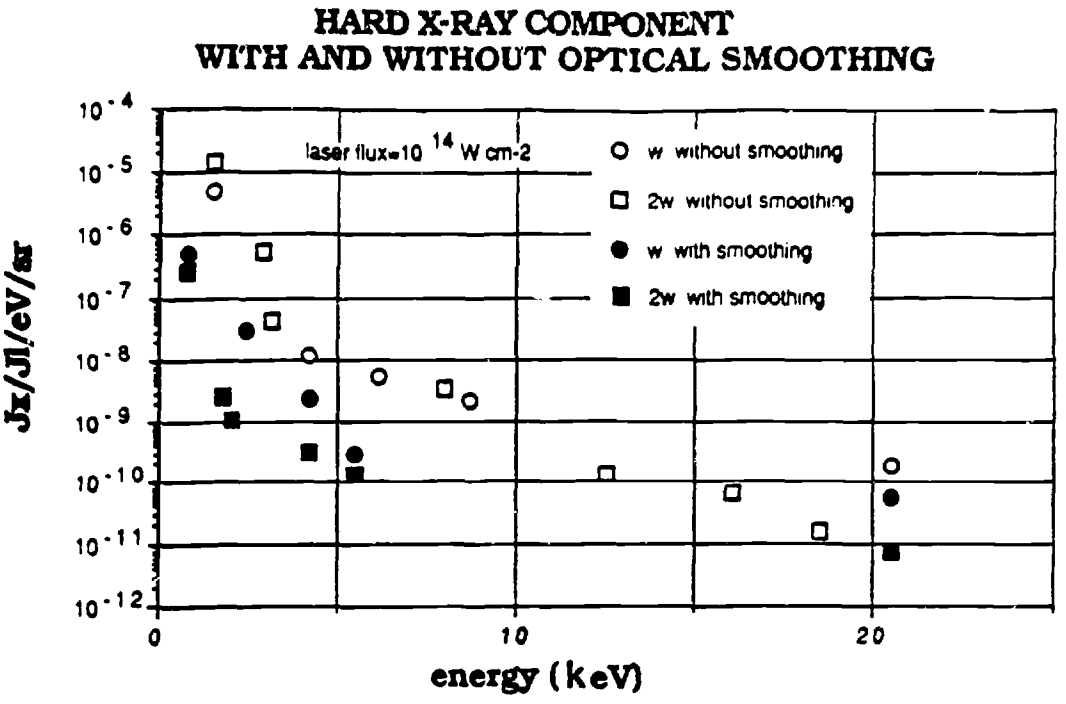

Fig. 7 Effect of optical smoothing at 1.06 and 0.53 µm on hard X-ray intensity

Exp OFO	Exp RPP	exp std	code
1.06µm 3.10^{15} W/cm^2 1ns			
110±10nm	110±10nm	110±10nm	30nm
0.53µm 10^{15} W/cm^2 1ns			
40±10nm			30-35nm
0.35µm 10^{14} W/cm^2 1ns			
	200±10nm	450nm	200nm

Fig. 8 Effect of optical smoothing by RPP and optical fibre oscillator, on ablation depth in a gold target

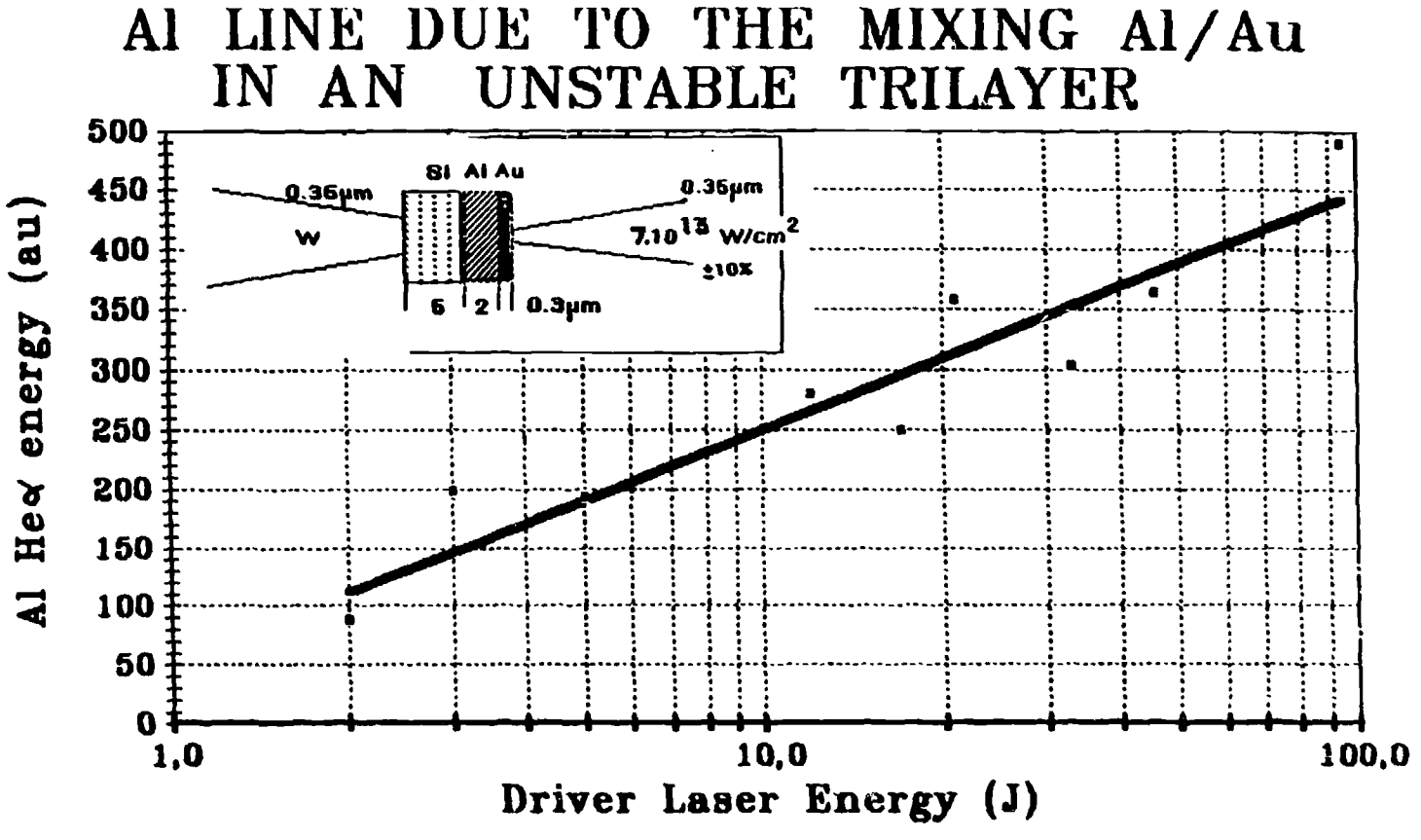

Fig. 9 Development of the mixing zone in a trilayer foil : variation of Al He_α line intensity versus the target acceleration

- we smoothed out the driver-beam non-uniformities and the probe-beam non-uniformities with "Random Phase Plates". The driver intensity could be varied from 10^{13} W/cm² to 5.10^{14} W/cm².
- the probe-beam features were : 0.35 µm instead of 1.06 µm; the focal spot was 120 µm FWHM which was smaller than the driver focal spot (200 µm) in order to probe only the center of the accelerated part of the foil. The intensity was $1\pm0.2\times10^{14}$ W/cm²; the probe depth measured was 0.2 ± 0.02 µm in the gold, that is, 2/3 of the total gold thickness instead of 1/3.

- the trilayers were basically the same as previously, but we used an anti-migration barrier between Al and Au at the rear of target.

- X-ray shadowgraphy and the X-ray emission due to the probe beam allowed us to determine the velocity of the foil and its acceleration: for 2.10^{14} W/cm² we measured 1.2×10^{7} cm/s and the acceleration deduced is about 10^{15} cm/s².

The first stage of this experiment was to check that, with some stable trilayer foils ,we do not detect any mixing between gold and aluminium and verify that the He_α Al line cannot be attributed to the ablation front instability induced by the driver beam at the front, or induced by the probe beam at the rear ; a typical stable trilayer can be constituted as following Au(0.5 µm)/Al(2 µm)/Si(1.5 µm) ; it is obtained by putting silicon instead of gold at the rear in order to present a very small density jump between Al and Si. Indeed, time resolved spectroscopy reveals that with such targets, the Al lines are delayed with respect to the Si lines by 600 ps which is compatible with the ablation of 1.5 µm of Si. Moreover the results obtained with stable trilayers allow us to fit our hydrocode with the main features of the motion of the foils.

In the second stage we confirmed that the the Al line appears for 1J (10^{13} W/cm²). In order to avoid the radiative preheating due to the gold, we used targets with a 5 µm Si front layer, and we found that the Al line intensity seems to grow as the logarithm of the driver energy (fig. 9).

Some trilayers foils with gold at the front were shot as in the first campaign, in order to find out what the real part of the preheating is ; the data processing is now under progress and the simulations as well.

2. PLASMA DIAGNOSTICS

Ref. 14 gives the diagnostic package implemented on Phebus and devoted to basic measurements routinely operating.

Other specific diagnostics have been devoted first to characterize the plasma emissions in the X-UV and soft X-ray ranges, second to measure the fuel density times radius $\langle \rho R \rangle$ and the fuel density-times thickness $\langle \rho \Delta R \rangle$ products at neutron emission peaks in I.C.F. experiments.

2.1. X-UV diagnostics

Three important diagnostics are now widely used in experiments where radiative transfer plays an important role :

- A streaked soft X-ray imaging system at $h\nu \approx 100$ eV (F.M.S.), constituted of an upgraded soft x ray streaked camera with both a temporal resolution better than 30 ps, and a spatial resolution of 8 lp mm^{-1}, associated with a flat SiO_2 mirror on grazing incidence as low band pass filter, a vertical slit for spatial resolution and a soft X-ray filter (typically 0,5 $mg.cm^{-2}$ of carbon).

- A transmission grating streaked soft X-ray high resolution spectrometer (SPARTUVIX), developed for soft X-ray laser studies [21], using a collecting optic, a transmission grating and a movable camera equipped with an optical fi ucial.

- A transmission grating streaked soft X-ray broad band spectrometer (SMART), built for spectral analysis between 40 eV and 1 keV. It is composed of a transmission grating (5000 Å period) which can be translated in order to adjust the spectral range of the diffracted spectrum into the fixed slit of the soft X-ray streaked camera (8 lp mm^{-1}, 30 ps). Fig. 10 shows a typical picture recorded during the interaction of a two beams shot of Phebus on a thin planar fold foil. We can see the time evolution of the diffracted soft X-ray spectrum emitted by the plasma, present on both sides of the zero order. The 44,7 Å absorption K edge of the carbon filter is clearly identified.

2.2. Neutron diagnostics

Two complementary diagnostics are developed to measure the performances of an ablative implosion :

. Fuel $\langle \rho R \rangle$ measurement by knock-on method

The neutron produced by the DT fusion reactions have a small probability to scatter off deuterium and tritium ions in the fuel. The number of such scattering events is directly proportionnal to fuel $\langle \rho R \rangle$ times the neutron yield ϕ_n. By counting the number of elastically scattered D and T ions (knock-on) and by measuring the neutron yield, it is possible to calculate the ρR value from the relation [22] :

$$\langle \rho R \rangle = 5.4 \frac{N_k}{\phi_n . \Omega . F} \quad (g.cm^{-2})$$

where ϕ_n is the neutron yield, N_k the number of detected knock-on particles in the solid angle Ω and in the detection energy window, and F a parameter depending on filters and film thick-

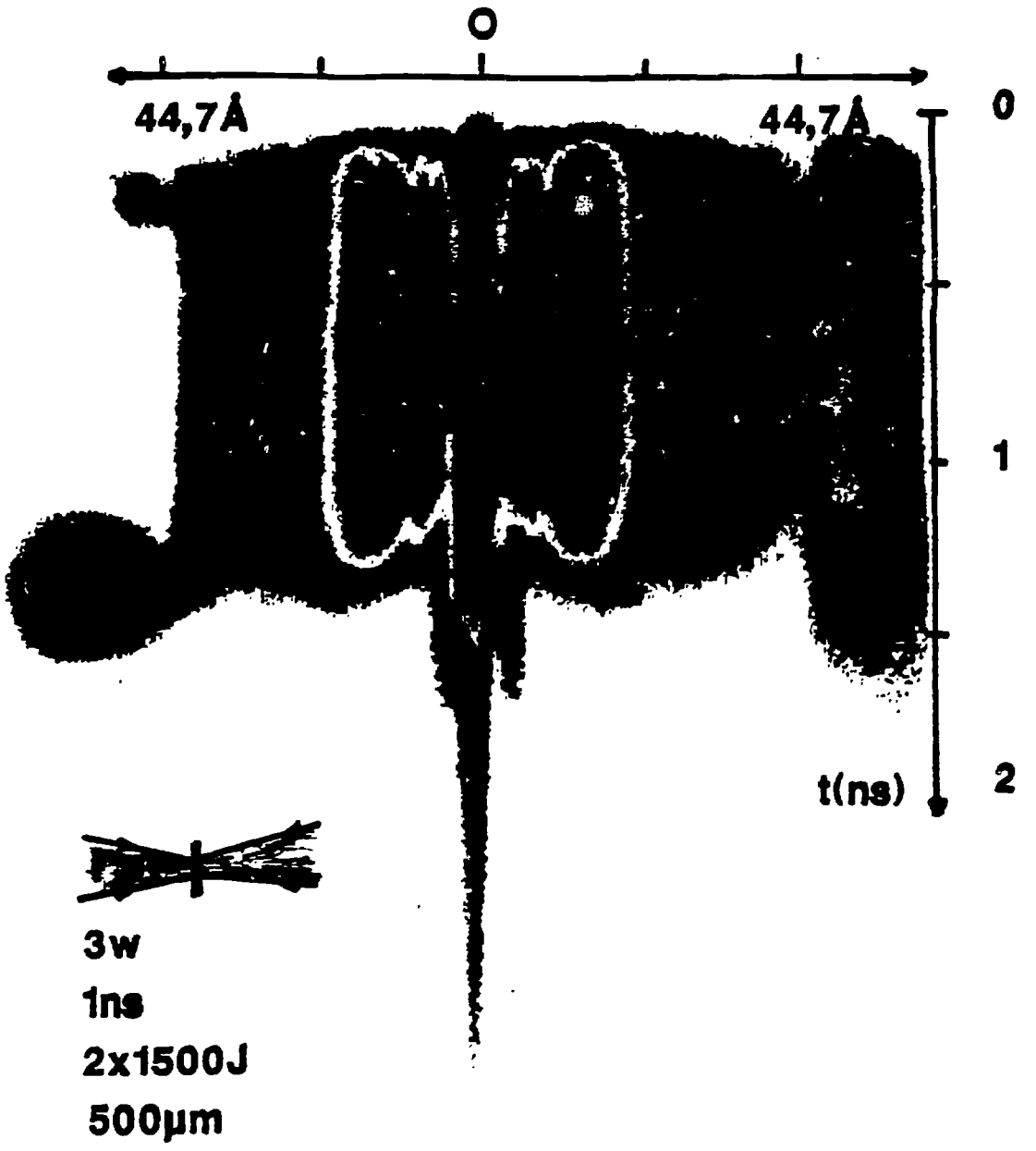

Fig. 10 Time evolution of the soft X-ray spectrum emitted from a planar gold target irradiated by the two laser beams of Phebus

nesses ; we used the solid state track detector CR 39 (150 µm in thickness) protected by tantalum. Identifying, counting and measuring the pits after etching of the CR 39 in a hot sodium hydroxyde solution being tedius, we have developed a computerized microscope system for an automated treatment. Being focused at the top of the detector, the system goes and seek for the coincidence tracks at the bottom surface by shifting the sample ; then it returns to the top and advances to the next location and begins a new stage of scanning. Identification and counting of knock-on tracks has been successfully tested on CR 39 irradiated in an accelerator.

. **Radiochemistry measurements**

In an imploded laser fusion target consisting of DT gas encapsulated in a glass microballoon, the 14,1 MeV neutrons activate the Si^{28} atoms in the glass via the nuclear reaction $Si^{28}(n,p)Al^{28}$. Knowing the neutron yield ϕ_n and the total number of Al atoms created, one can find the areal density $\langle \rho, \Delta R \rangle$ of the compressed glass shell at the time of peak neutron production [23]. The method uses a highly efficient (4 π sr) beta-gamma coincidence and low noise (0.3 count.min^{-1}) detector, and a fast extraction target-debris collection system shown on fig. 11. The debris collector is a conical titanium foil (5 cm in diameter, 10 cm length) located 1 cm apart from the target. To increase the collection rate, a dish shaped tantalum reflector is placed in opposite situation, at a distance 2.5 cm from the target. The automated system takes 25 seconds to transfer the collector from the chamber to the counting system. Before a shot, microballoons are made slightly radioactive by thermal neutron irradiation, which creates the Na^{24} isotope of sodium included in the glass. The fraction of target debris which have been collected is determined from the ratio of Na^{24} activity found on the collector, to that initially measured in the target. The system that we have developed should be able to measure $\phi_n \langle \rho, \Delta R \rangle \geq 1.3\ 10^5$ g.cm^{-2}.

3. LASER RESEARCH

The Centre d'Etudes de Limeil-Valenton in France is involved in solid-state laser research since the very beginning in 1966. Together with the "Compagnie Générale d'Electricité" we developed successively several laser facilities experiments. Two of them are still employed : P102, a single beam laser delivering about 100 joules at 1.06 µm in a 1 ns pulse duration, and OCTAL which is an eight beam laser delivering a total energy of 2 kilojoules at 1.05 µm in a 1 ns pulse duration or about 600 joules after frequency conversion at 0,35 µm.

More recently, using the technology developed by the Lawrence Livermore National Laboratory in the U.S., we built a two arm-power laser, PHEBUS, able to produce routinely 15 kJ at 1.05 µm and 5 kJ at 0.35 µm in 1 ns on target.

In order both to operate and maintain such facilities, and to improve their performances, several projects in research and development areas are supported.

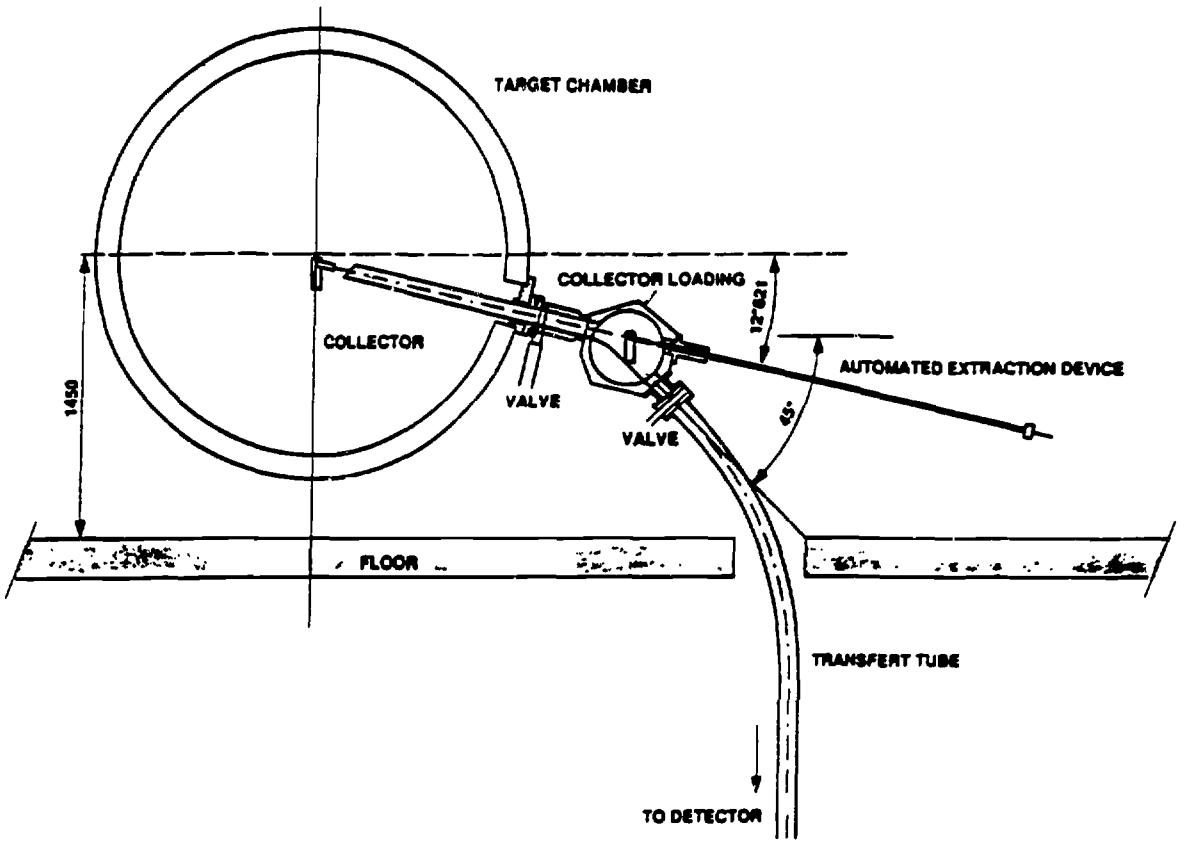

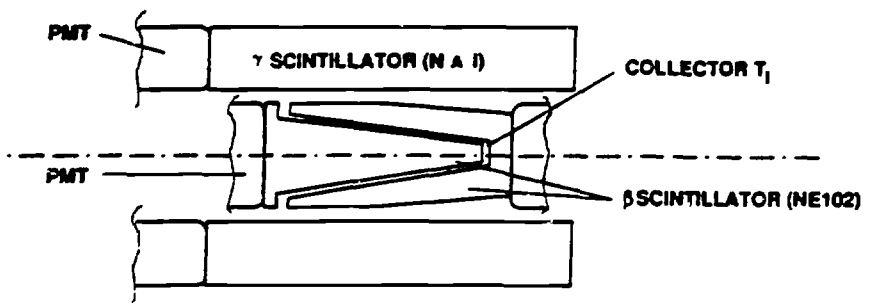

Fig. 11 Scheme of the fast extraction target debris collection system and of the 4 π βγ detector for radiochemistry measurements

3.1. Optical smoothing

The first one concerns a beam smoothing technique which can be used to improve the uniformity of target illumination which is particularly important in the case of direct drive irradiation of targets.

The laser beam produced by a wide band (≈ 3 nm) oscillator is introduced into a step index multimode optical fibre right after it comes out of the oscillator [6]. At the output of the fibre, each mode created a conical photon layer, which transit time depends on the cone angle. When focused, the beamlets are producing successive independent interference patterns with an individual life time no longer than the coherence time. Therefore, many different patterns superimpose during the pulse duration. The temporal dispersion of photons entering the multimode fibre with different angles of incidence is illustrated fig. 12a. It is clear that the path length increases with increasing angles and the photons present at the same time at the fibre entrance are experiencing various delays upon travelling along the fibre. Only discrete values of θ corresponding to the propagation modes of the fibre have to be considered. The number of modes N that can propagate, assuming that the incident beam is linearly polarized [24], is more than 300 for the following conditions :

- fibre diameter : 100 µm
- fibre length L : 50 m
- numerical aperture θ : 0.12
- wavelength : 1 µm

The maximum time delay d experienced by the outermost incident rays with respect to a ray with nul incidence is such as :

$$d = L\,\theta^2 / 2\,n\,c$$

where c is the speed of light, and n the refractive index. With n = 1.5 and the above values : d ≈ 1.5 ns. Then, the mean delay between each mode is of the order of 3 ps. it is larger than the 1 ps coherence time of the laser pulse and the condition for efficient smoothing is fulfilled. The beam is then focused near the input end of the fibre. The pulse emerging from the fibre output end is injected into a silicate glass rod amplifying chain. The image of the fibre output is relayed throughout the chain with the help of adequat optics and beam expanders. The beam is finally focused with a 600 mm focal length lens which forms a 300 µm diameter image of the fibre output. The maximum laser energy is about 70 J.

Spectroscopic measurements show that the width of the sepctrum is constant over the whole laser chain, thus demonstrating that the amplification of the wide band pulse is not selective. This observation is of importance since the smoothing efficiency relies on the spectral width. Spectral narrowing occurs only after frequency conversion (fig. 12b). The focal spot is dramatically improved at the fundamental frequency : the intensity profile has sharp edges and residual oscillations are smaller than ± 10 %. At the second harmonic,

the profile is even smoother, but due to the principle of frequency conversion, it is more peaked. At the third harmonic, the measured profile is perturbed by the strucutre of the CCD camera. By placing a square hole in an image plane of the fibre output, a square focal spot has been obtained at the fundamental frequency. At higher harmonics, the square shape vanishes. These results are summarized in fig. 13.

Frequency conversion has been conducted with an assembly of two type II, 16 mm thick, KDP crystals in the quadrature configuration. An efficiency close to 40 % has been reached for frequency doubling, and 12 % for tripling. Although in this last case, the characteristics of the KDP's are not optimized, the spectral width of the beam is probably responsible for a large part of this relatively low value.

Efficient smoothing has been obtained by the optical fibre technique. Further study of frequency conversion, mainly at the third harmonic, is needed. Although no evidence of self focusing in the amplifier rods has been detected, this phenomenon deserve to be investigated in order to determine how it can be influenced by smoothing at the front end [25].

3.2. Reflective sol-gel coatings from colloïds

A second subject concerns new techniques able to produce antireflection or mirror coatings able to support higher fluences than the classical Physical Vapour Deposition techniques generally used, we have been investigating the sol-gel technique in synergy with LLNL [26]. In this process, a suitable ionic or molecular precursor solution leaves an inorganic film residue when applied and evaporated. After an extensive work carried out at CEL-V and else we have learned that the best method consisted in an application of a colloidal suspension of a chemically converted oxide to a substrate with subsequent evaporation of the suspending medium.

We have prepared at room temperature optical-coatings of high-index oxide materials such as ; TiO_2, ZrO_2, HfO_2, ThO_2 and Al_2O_3, H_2O deposited from colloidal suspensions. All these films were porous and consequently of low refractive index compared to the relevant dense material. This prospective work revealed Al_2O_3, H_2O as the more laser damage resistant high-index oxide candidate (Fig. 14).

Alternating these high-index components with early reported SiO_2 also deposited from a colloidal suspension we were able to prepare highly reflective coatings at room temperature (Fig. 15). Among the different oxide combinations, the AL_2O_3-SiO_2 system appeared to be the strongest in laser-resistance, conserving its performances compared to those of the original constituing components when prepared in stringently clean conditions.

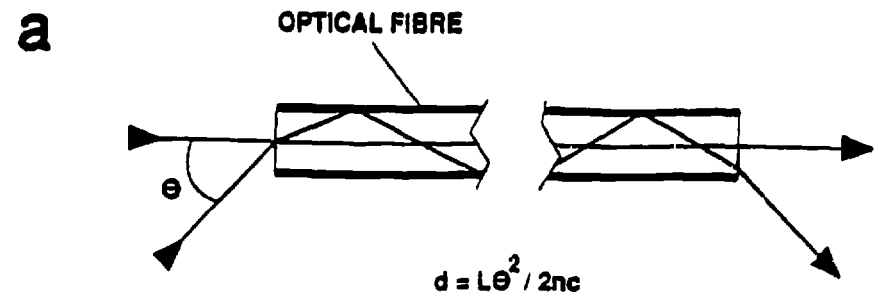

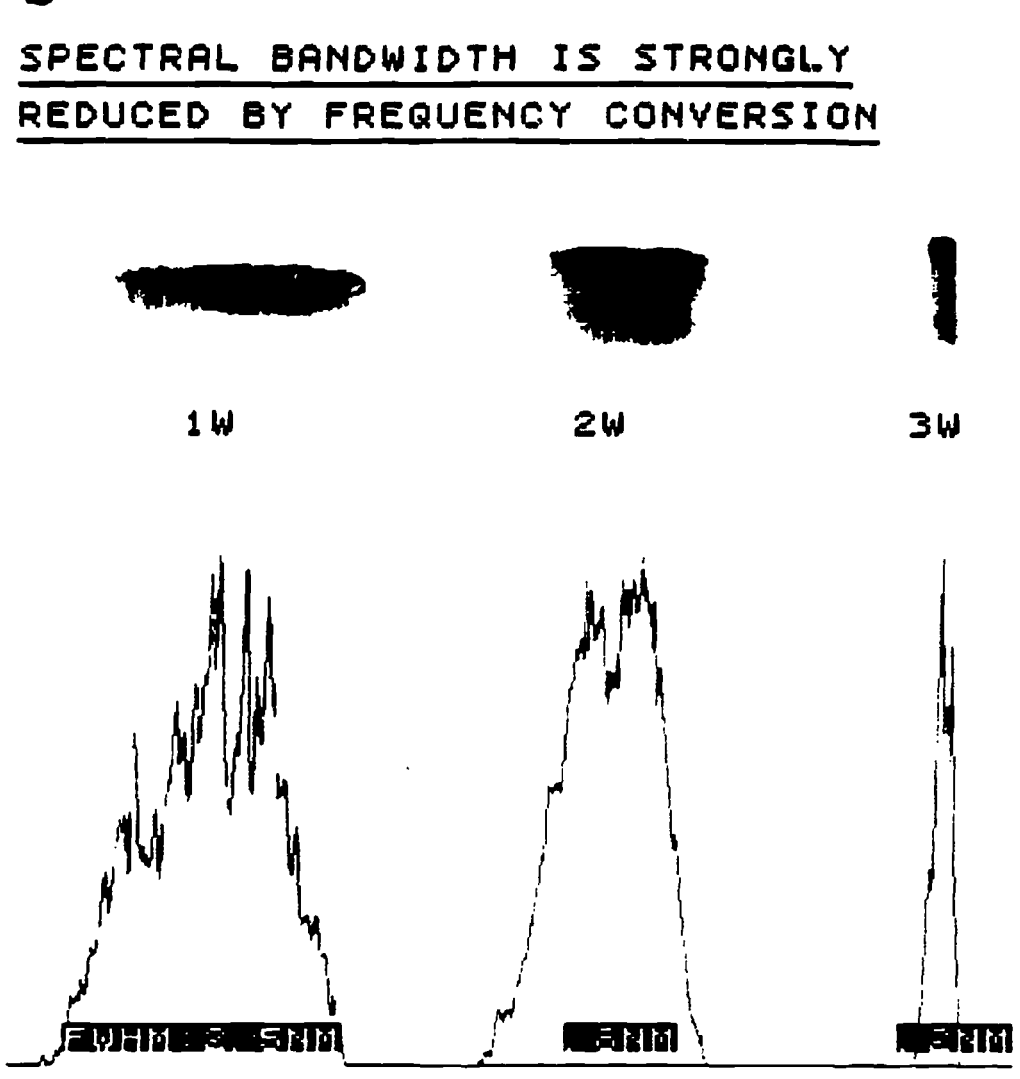

Fig. 12 - Optical fibre dispersor (a)
The ray entering the fibre with an angle of incidence θ is delayed by an amount d with respect to the ray parallel to the fibre axis.

- Laser pulse spectra (b)
The spectral width is reduced after frequency conversion.

FOCAL SPOT PROFILES ARE MODIFIED BY FREQUENCY CONVERSION

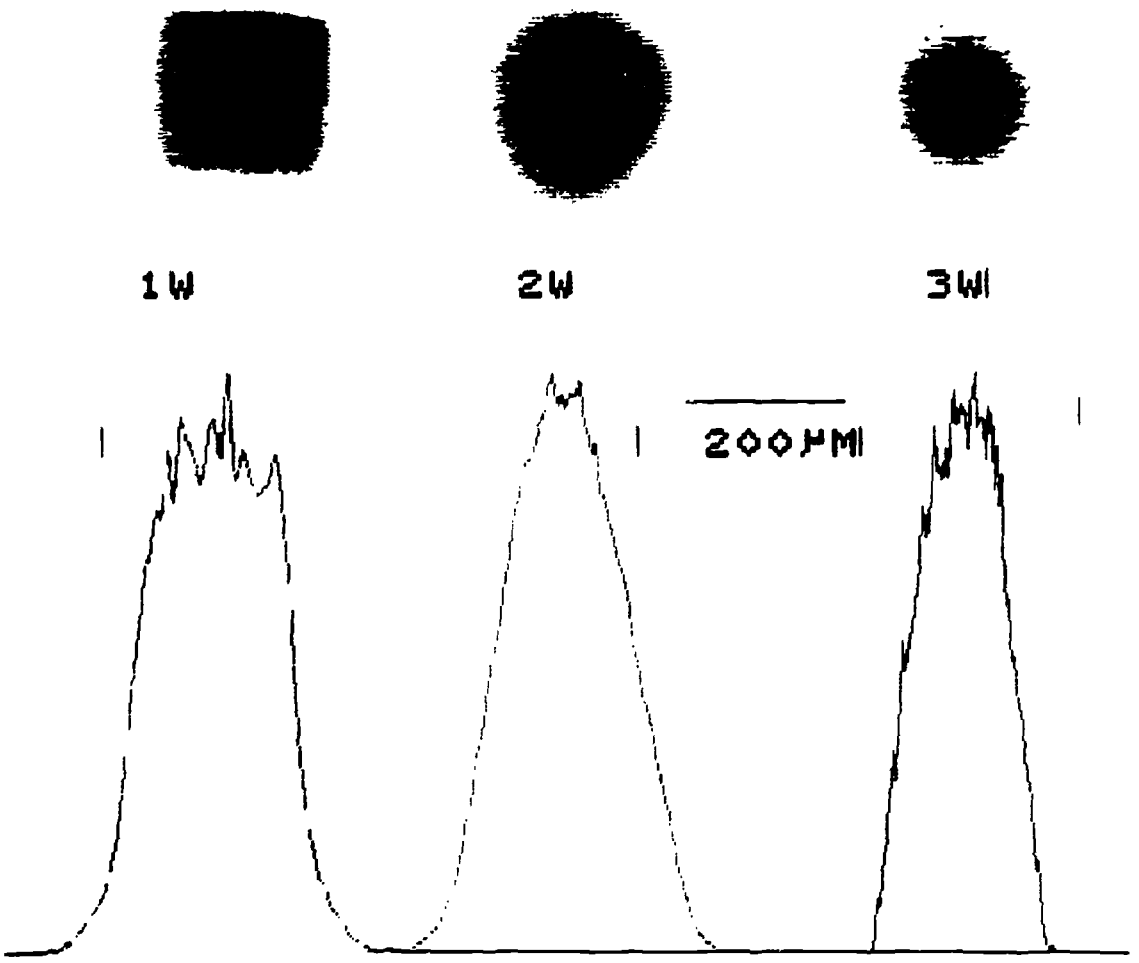

Fig. 13 - The square focal spot
This focal spot is obtained by imaging a 2x2 mm² square aperture placed in an image plane of the fibre end. The square shape, (200 µm)² , obtained at the fundamental frequency, vanishes at higher harmonics. At the third harmonic, the poor sensitivity of the camera leads to profile irregularities due to the CCD structure.

OXYDE	INDEX	DAMAGE AT 1064 nm.J/cm2		
		1ns, SINGLE SHOT	10ns, SINGLE SHOT	10ns, 30Hz
SiO2	1.20	14 - 15	30 - 40	30 - 40
Al2O3.H2O	1.43	11 - 14	30 - 40	40
ZrO2	1.48	7 - 10	10 - 20	10 - 15
HfO2	1.50	8 - 11	15 - 20	15 - 20
TiO2	1.80	8 - 10	15 - 20	2 - 5
ThO2	1.50	10 - 13	20 - 25	?

Figure 14 Damage thresholds of single-coatings

OXYDE-PAIR	DAMAGE AT 1064 nm.J/cm2		
	1ns, SINGLE SHOT	10ns, SINGLE SHOT	10ns, 30Hz
TiO2-SiO2	6 - 8	10	1 - 4
ZrO2-SiO2	6 - 7	10 - 15	10
HfO2-SiO2	5 - 8	15	15
ThO2-SiO2	8 - 9	20	?
Al2O3-SiO2	8 - 13	30 - 45	25 - 48

Figure 15 Damage thresholds of HR-coatings

CONCLUSION

The laser research and development program at Centre d'Etudes de Limeil-Valenton is concentrated on high performances ablative implosions. The indirect drive scheme has been chosen as the most promising approach towards the I.C.F. objective. It involves a deep study of key subjects such as radiative transfert, fuel preheat and hydrodynamic instabilities, and a concomitant effort on plasma diagnostics and high power laser advanced technology.

REFERENCES

1. J. Nuckolls, L. Wood, A. Thirsen, G. Zimmermann
   Nature (London) 239, 139 (1972)
2. R.H. Lemberg, S.P. Obenschain
   Opt. Comm. 46, 27 (1983)
3. S. Bodner et al.
   12th International Conference on Plasma Physics and Controlled Nuclear Fusion Research, Nice, France, (1988)
4. Y. Kato et al.
   Phys. Rev. Lett. 53, 1057 (1984)
5. R.L. McCrory et al.
   12th International Conference on Plasma Physics and Controlled Nuclear Fusion Research, Nice, France, (1988)
6. D. Veron et al.
   Opt. Comm., 65, 42 (1988)
7. J.M. Soures
   30th APS Meeting, Division of Plasma Physics
8. J. Kilkenny et al.
   12th International Conference on Plasma Physics and Controlled Nuclear Fusion Research, Nice, France, (1988)
9. B. Meyer, G. Thiell
   Phys. of Fluids, 27, 302 (1984)
10. K. Nishihara
    Jap. Journ. of App. Phys. 21, 1571 (1982)
11. J. Meyer Ter Vehn et al.
    Phys. Lett., 104, 410 (1984)
12. M. André et al.
    12th International Conference on Plasma Physics and Controlled Nuclear Fusion Research, Nice, France, (1988)
13. Laser Interaction and Related Plasma Phenomena
    Vol. 8, p. 817, Plenum Press, New York, 1984
14. Laser Interaction and Related Plasma Phenomena
    Vol. 8, p. 503, Plenum Press, New York, 1988
15. J.L. Bocher et al.
    P.R.L. 52, n° 10 (1984), 823
16. D. Veron et al.
    Opt. comm. 65, (1988), 42
17. R.A. Bosch et al. (KMS.F) ; D. Kania, P. Bell (LLNL)
    APS Meeting, Division of Plasma Physics, 1988
18 S.P. Obenschain et al
    P.R.L. 62, 7 (1989) 768

19. P.A. Holstein et al
Anomalous Absorption Conf., June 1989
20. P.A. Holstein et al.
C.R. Ac. Sc. 307 (1988), 211
21. J.L. Bourgade et al.
Rev. Sci. Instr. 59, 8 (1988), 1840
22. S. Kacenjar et al.
P.R.L. 49, 7 (1982), 463
23. E.M. Campbell et al.
J.A.P. 51, 12 (1980), 6062
24. D. Gloge
App. Opt. 10 (1971) 2252
25. A.A. Max et al.
Sov. Tech. Phys. Lett. 6, 2 (1970)
26. H.G. Floch, J.J. Priotton, J.M. Thomas
The physics and technology of amorphous silica
Plenum Press 561 (1988)

FIGURE CAPTION

Fig. 1 Time-integrated X-ray pictures of core emission from X-ray driven implosions

Fig. 2 X-ray conversion efficiency and front emission lobe from planar thick gold targets

Fig. 3 Main features of rear side X-ray emission from thin gold targets ($e < 1$ µm)

Fig. 4 Compared experimental data and numerical simulation of rear side X-ray emission for planar gold layers ($e > 1$ µm)

Fig. 5 Hydrodynamical behaviour of a laser irradiated thin gold target. Streaked soft X-ray recording ; superimposed 1D numerical simulation

Fig. 6 X-ray emission from gold targets irradiated with a smoothed beam : front emission lobe and conversion efficiency compared with non-smoothed beam results

Fig. 7 Effect of optical smoothing at 1.06 and 0.53 µm on hard X-ray intensity

Fig. 8 Effect of optical smoothing by RPP and optical fibre oscillator, on ablation depth in a gold target

Fig. 9 Development of the mixing zone in a trilayer foil : variation of Al He_α line intensity versus the target acceleration

Fig. 10 Time evolution of the soft X-ray spectrum emitted from a planar gold target irradiated by the two laser beams of Phebus

Fig. 11 Scheme of the fast extraction target debris collection system and of the $4\pi\beta\gamma$ detector for radiochemistry measurements

Fig. 12 - Optical fibre dispersor (a)
The ray entering the fibre with an angle of incidence θ is delayed by an amount d with respect to the ray parallel to the fibre axis.

- Laser pulse spectra (b)
The spectral width is reduced after frequency conversion.

Fig. 13 - The square focal spot
This focal spot is obtained by imaging a 2x2 mm^2 square aperture placed in an image plane of the fibre end. The square shape, $(200\ \mu m)^2$, obtained at the fundamental frequency, vanishes at higher harmonics. At the third harmonic, the poor sensitivity of the camera leads to profile irregularities due to the CCD structure.

Fig. 14 Damage threshold of single coatings

Fig. 15 Damage threshold of HR coatings

I. C. F. PROGRAM

at

CENTRE D'ETUDES DE LIMEIL-VALENTON

I.C.F. Program at CEL-V

- AT CEL-V, WE PERFORM EXPERIMENTS WITH THE INDIRECT-DRIVE SCHEME : IN A HOHLRAUM, THE LASER ENERGY IS CONVERTED TO X-RAYS WHICH IMPLODE A SPHERICAL CAPSULE.

- THIS PROGRAM INVOLVES STUDIES OF KEY ISSUES : RADIATIVE TRANSFERT AND PREHEAT, HYDRODYNAMICS INSTABILITIES, SYMMETRY OF DRIVE.

- ACCOMPANYING EFFORT IS DEVELOPED ON DIAGNOSTICS AND ADVANCED LASER TECHNOLOGY.

RADIATION DRIVEN IMPLOSIONS : UNIFORMITY

- HIGH YIELD IMPLOSION REQUIRE A HIGH DEGREE OF DRIVE ENERGY UNIFORMITY (TYPICALLY 1%)

- THE DIRECT DRIVE APPROACH NEEDS SMOOTHING TECHNIQUES SUCH AS ISI - OR RELEVANT METHODS - ,RPP, OR BEAMS OVERLAPPING.

  BEST RESULT TO DAY AT LLE : 10% RMS

- THE INDIRECT DRIVE SCHEME CAN ENHANCE THE UNIFORMITY WHITH LESSER CONSTRAINTS ON BEAMS NUMBER AND QUALITY
  3% AT LLNL

- UNIFORMITY CAN BE IMPROVED BY A PROPER CHOICE OF HOHLRAUM GEOMETRY

INDIRECT DRIVE IMPLOSION EXPERIMENTS AT CELV

The implosion symmetry is controlled by varying hohlraum geometry

Core X-ray emission is observed :

for two Laser beams , versus hohlraum geometry

b/a = 2.5 | b/a = 2.7 | b/a = 1.6 | b/a = 1.3

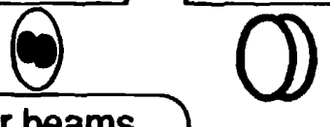

for eight Laser beams

b/a = 1.1

1 DIM

$\Delta R / R = 20\ \%$

RADIATION DRIVEN IMPLOSION : ENERGY REQUIREMENT

- AN IRRADIATION DEFECT CAN PREVENT A HIGH RADIAL CONVERGENCE OF AN IMPLODING SHELL, EVEN BEFORE BREAKING UP BY R.T. INSTABILITIES

  CONSEQUENTIAL EFFECT ON ENERGY REQUIREMENT CAN BE ROUGHLY ESTIMATED FOR BOTH DIRECT (D) AND INDIRECT (I) SCHEMES.

- PUSHER VELOCITY : $V = \alpha\, PA/\dot{M}$

  $PA/\dot{M} = \alpha' \Phi^{k}$

DIRECT DRIVE $k_D = 1/3$ - FOR EXPLE
B. MEYER - G. THIELL
PHYS OF FLUIDS
27 (1984) 302

INDIRECT DRIVE $k_i = 0.17$ - K. NISHIHARA
JAP. J. OF APPL. PHYS
21 (1982) 1571

- J. MEYER TER VEHN
PHYS LETT. 104 (1984) 410

RADIATION DRIVEN IMPLOSIONS : ENERGY REQUIREMENT

(cont'd)

• AN INITIAL IRRADIATION DEFECT $\Delta\Phi$ PRODUCES A VELOCITY DEFECT

$$\frac{\Delta V}{V} = k \frac{\Delta \Phi}{\Phi}$$

RELATIVE DEFECT OF SPHERICITY AT TIME $T_F = Ro/V$:
(DISREGARDING SLOWING DOWN AND INSTABILITIES)

$$\frac{\Delta R}{R} = \frac{Ro}{R} k \frac{\Delta \Phi}{\Phi}$$

ALLOWING $\Delta R/R = 1/6$ (HALF THE FINAL VOLUME PERTURBED)

$$\frac{\rho_F}{\rho_o} = \frac{4.6\ 10^{-3}}{k^3} \left(\frac{\Phi}{\Delta \Phi} \right)^3$$

RADIATION DRIVEN IMPLOSIONS : ENERGY REQUIREMENT

(cont'd)

• THE ENERGY TO INVEST SCALING AS ρ_F^{-2} , η BEING

THE EFFICIENCY OF LASER ENERGY TRANSFER TO THE FUEL, WE GET

$$\frac{E_D}{E_I} = \frac{\eta_i}{\eta_D}\left(\frac{k_D}{k_i}\right)^6$$

FOR SAME INITIAL IRRADIATION DEFECT

SAME FINAL CORE DEFECT

• ASSUMING $\frac{\eta_i}{\eta_D} = 0.1$ $E_D/E_I = 6$

RADIATIVE TRANSFER

- X-RAY EMISSION IN HIGH Z PLANAR TARGETS HAS BEEN WIDELY STUDIED :

  CONVERSION EFFICIENCY

  SPECTRA

  LOBE

  EVOLUTION IN TIME

  AS A FUNCTION OF IRRADIATION PARAMETERS (λ , Φ, Δ T)
  AND TARGET CHARACTERISTICS (MATERIAL, THICKNESS)

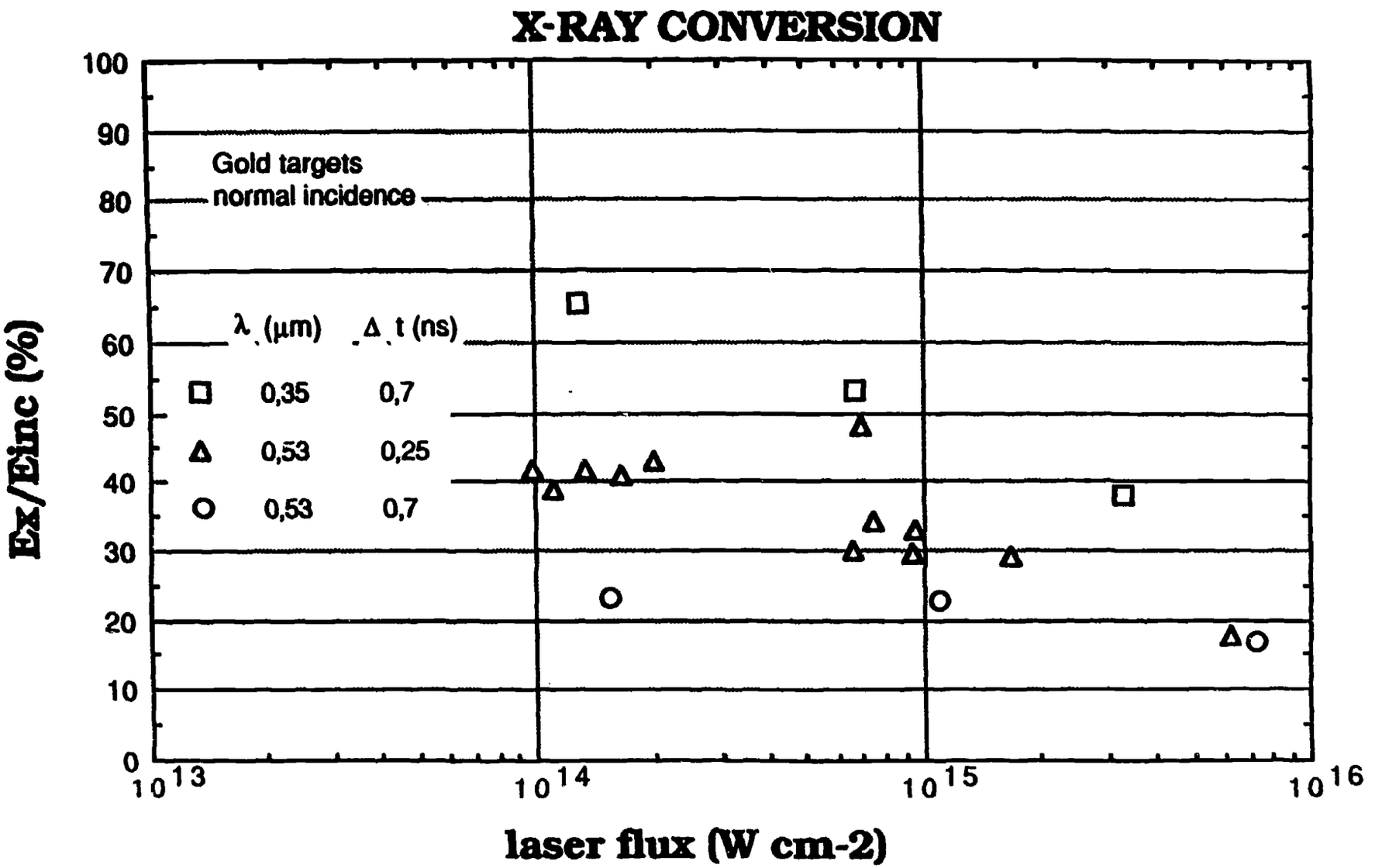
X-RAY CONVERSION
Gold targets
normal incidence
λ (μm)
Δ t (ns)
0,35
0,7
0,53
0,25
0,53
0,7
Ex/Einc (%)
laser flux (W cm-2)
100
90
80
70
60
50
40
30
20
10
0
10 13
10 14
10 15
10 16

FRONT EMISSION LOBE
gold plane target

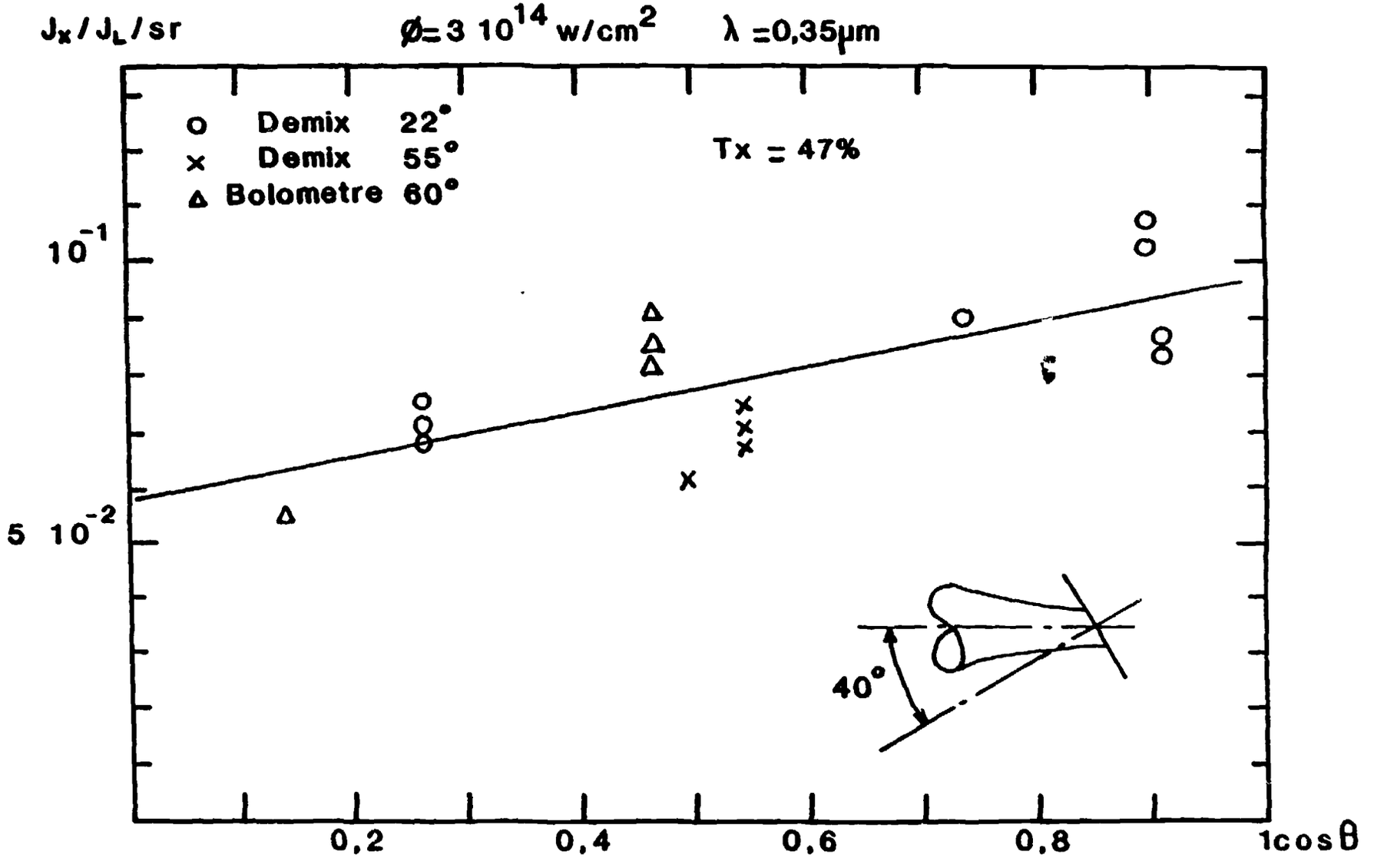

X-RAY CONVERSION EFFICIENCY
rear side ; gold target ; 0,35µm

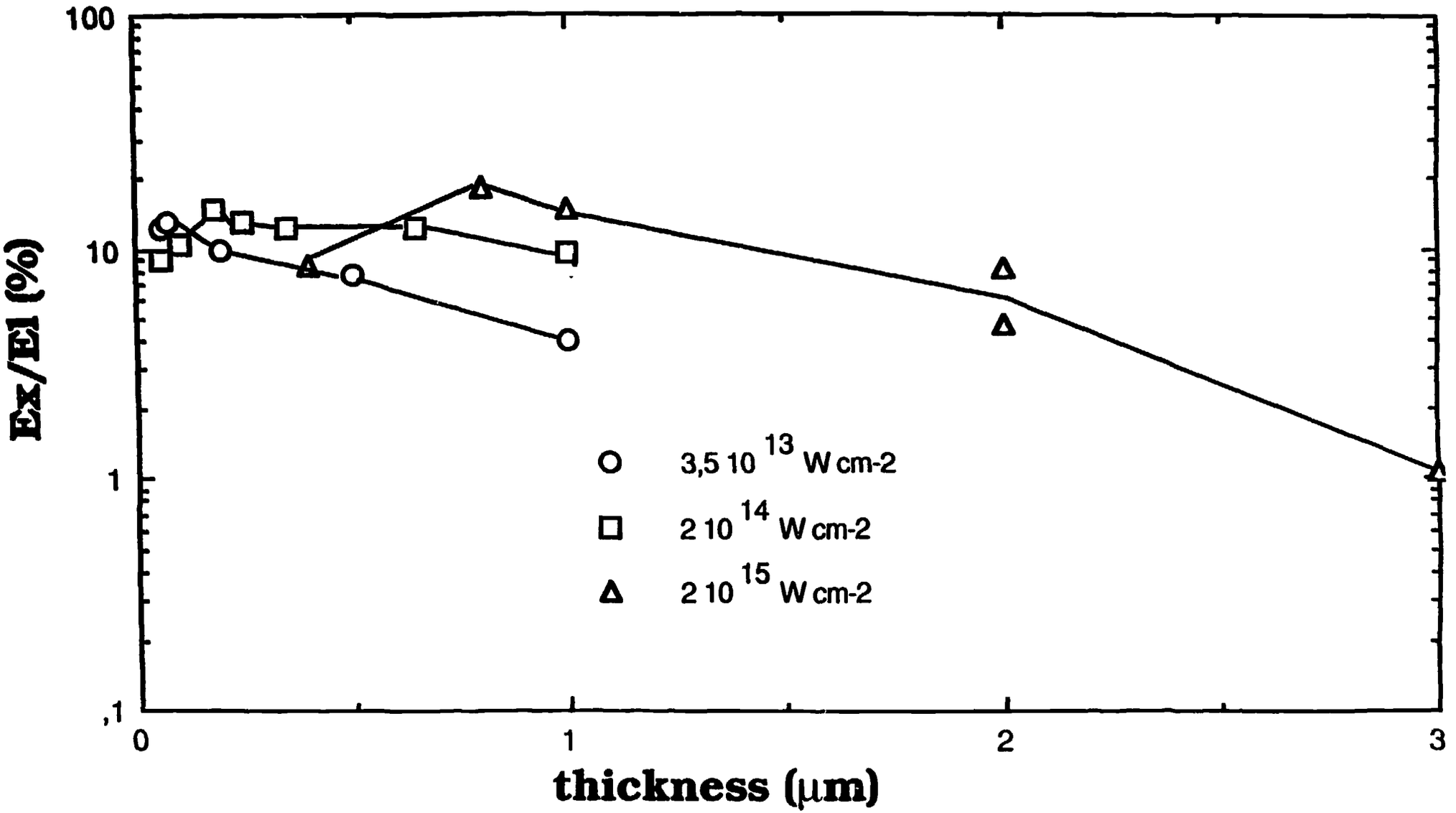

OPTIMAL THICKNESS FOR REAR SIDE X-RAY CONVERSION EFFICIENCY

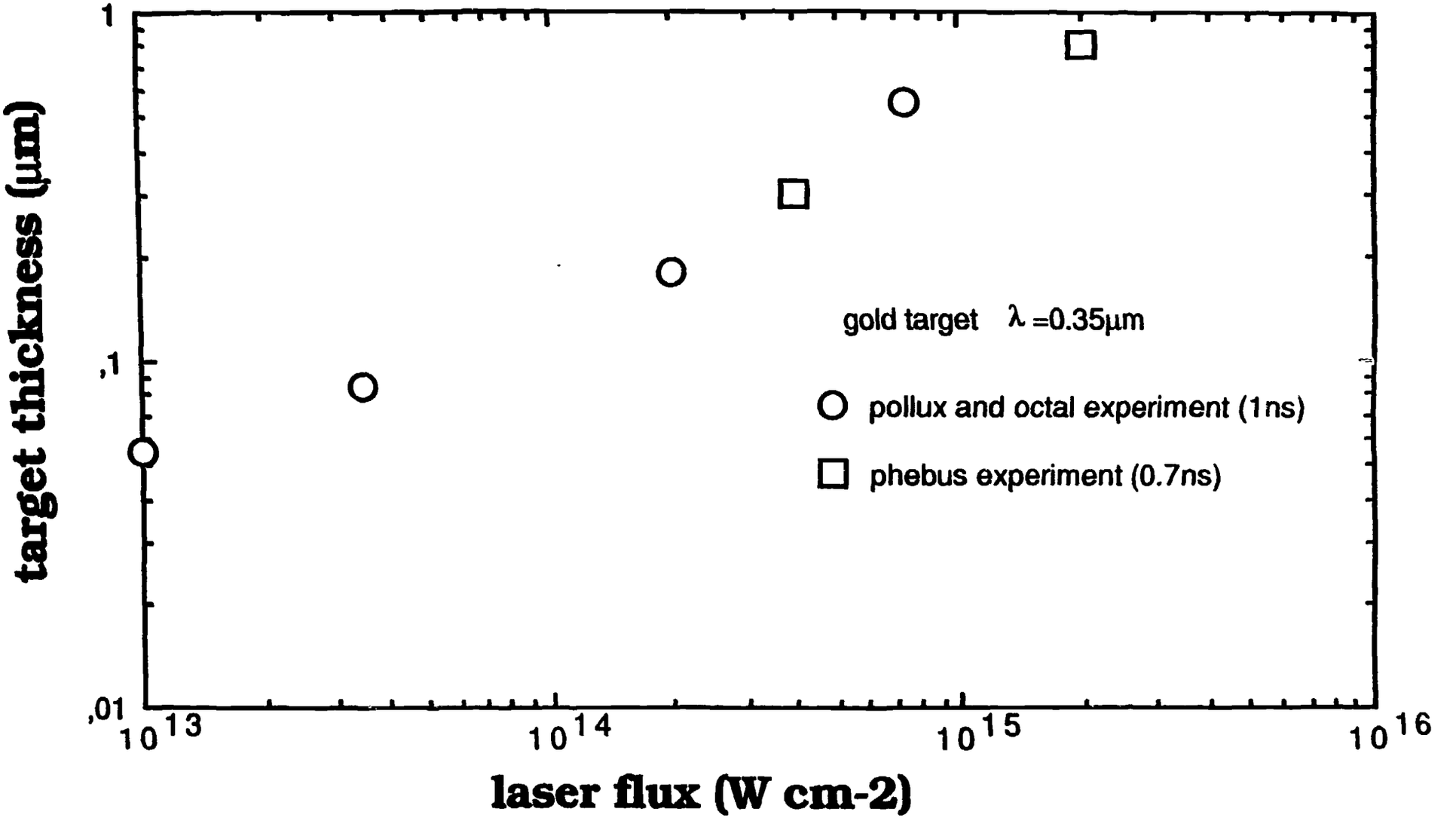

X-RAY CONVERSION EFFICIENCY VERSUS TARGET THICKNESS : EXPERIMENTS AND FCI-1 CODE

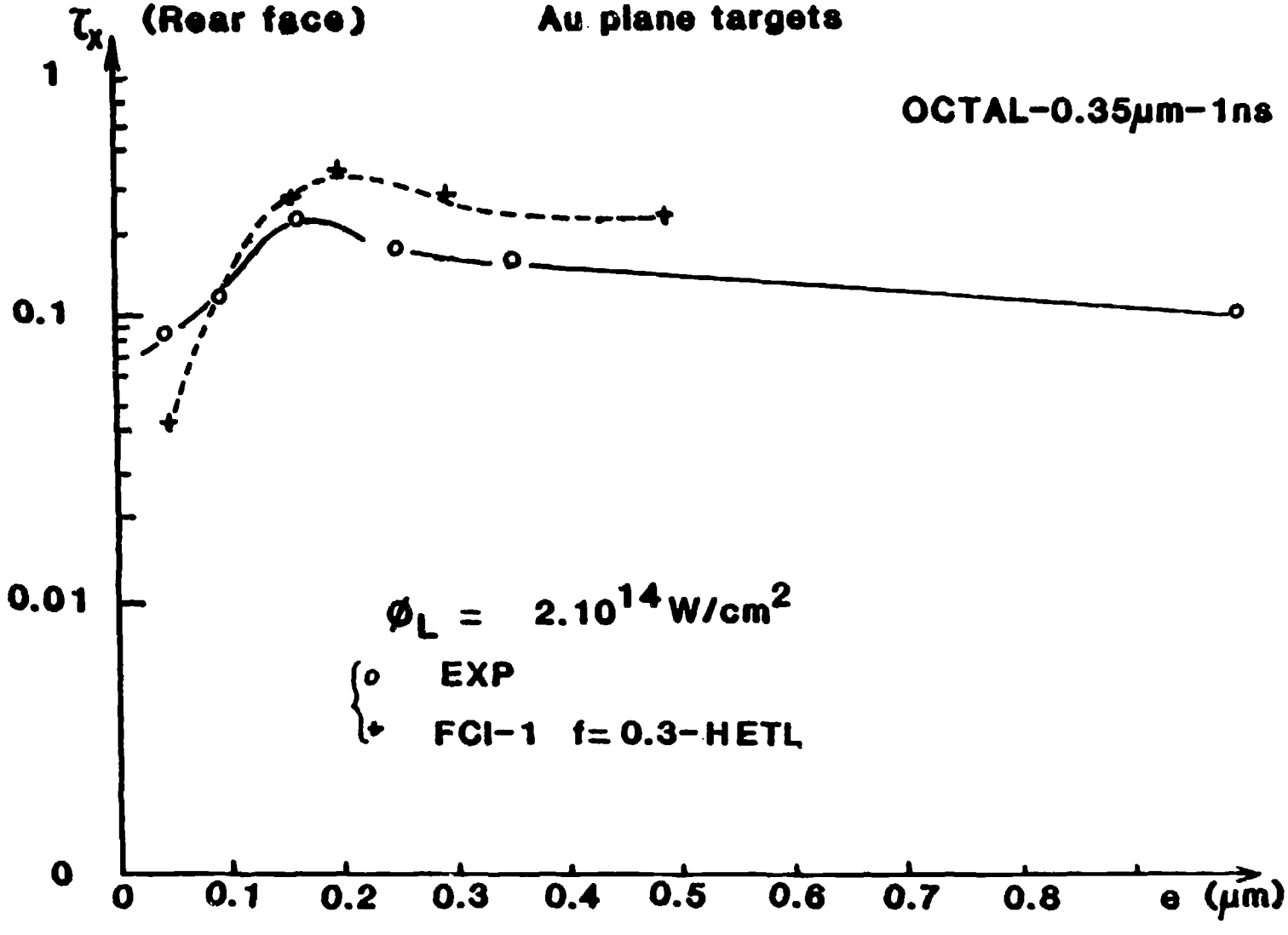

X-RAY CONVERSION WITH GOLD
normalized rear side emission versus thickness

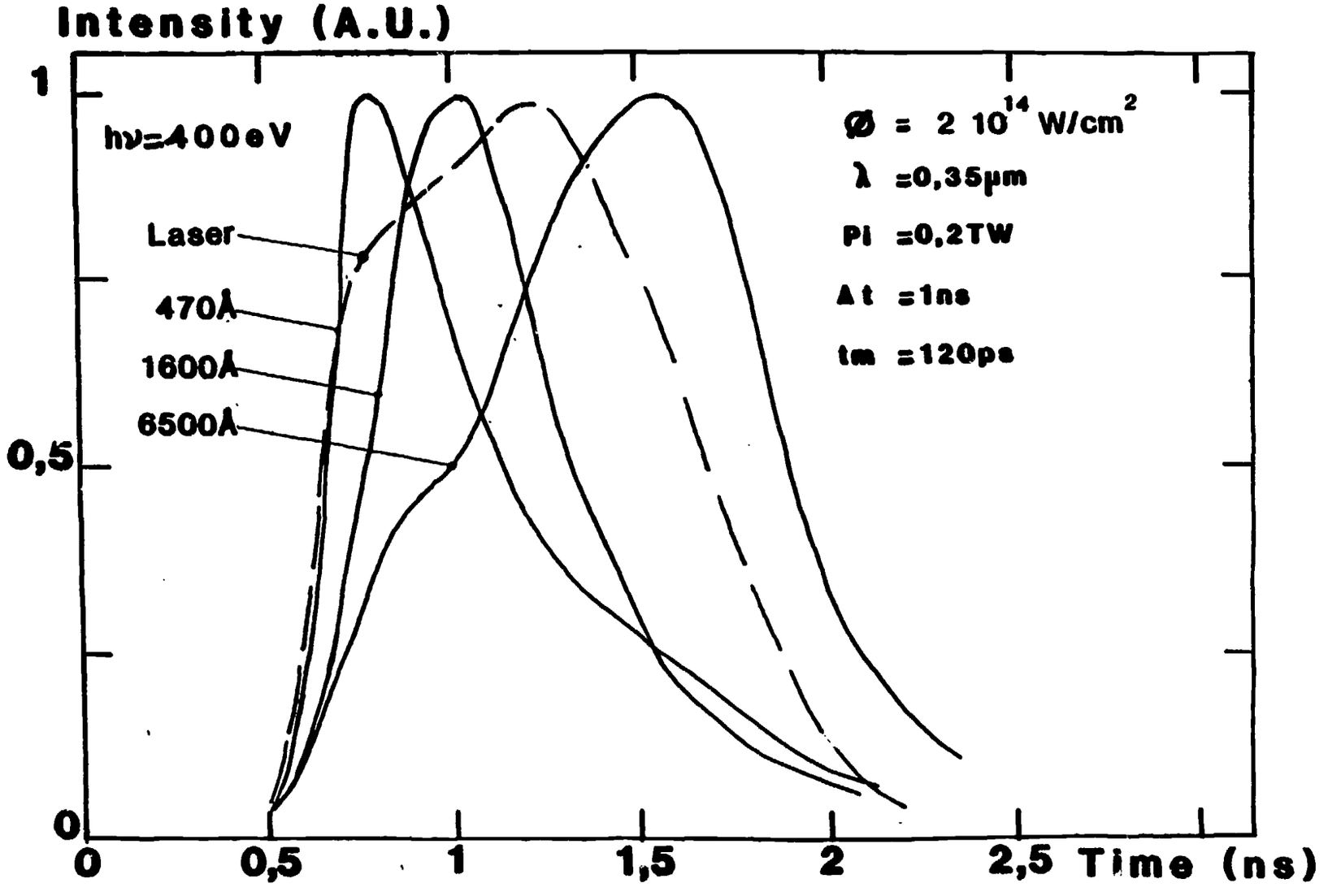

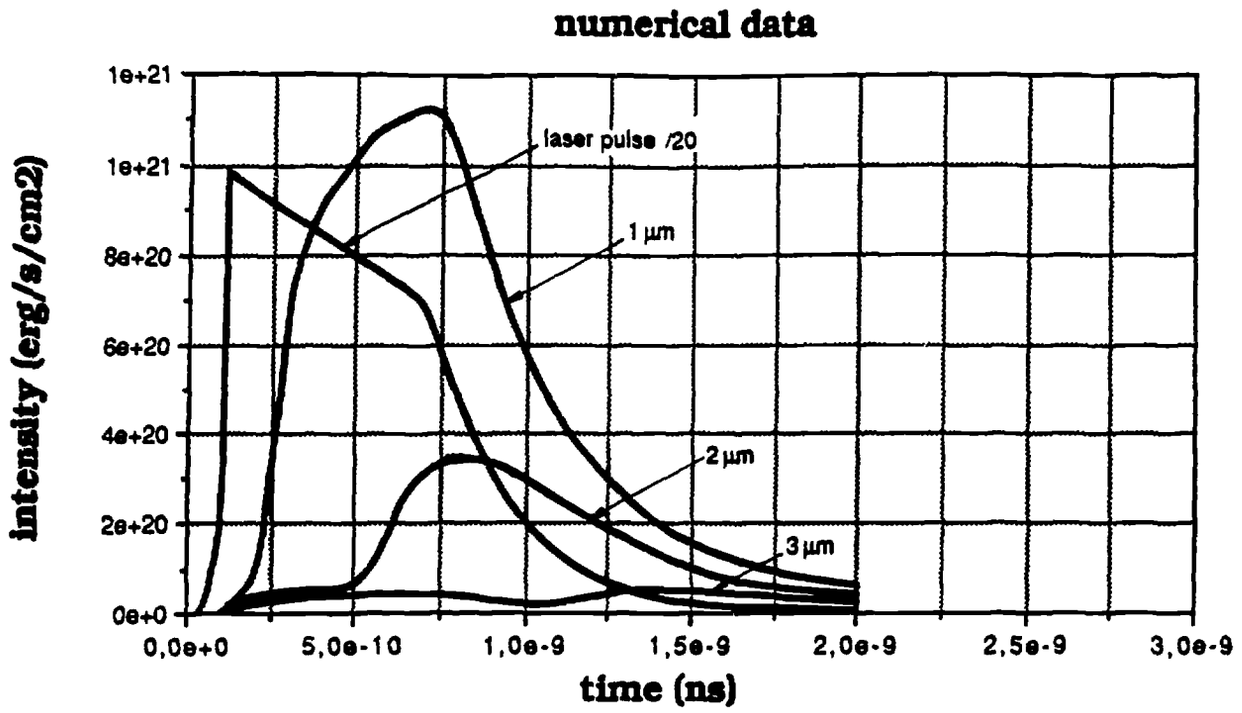
numerical data
intensity (erg/s/cm2)
1e+21
1e+21
8e+20
6e+20
4e+20
2e+20
0e+0
laser pulse /20
1 µm
2 µm
3 µm
0,0e+0
5,0e-10
1,0e-9
1,5e-9
2,0e-9
2,5e-9
3,0e-9
time (ns)

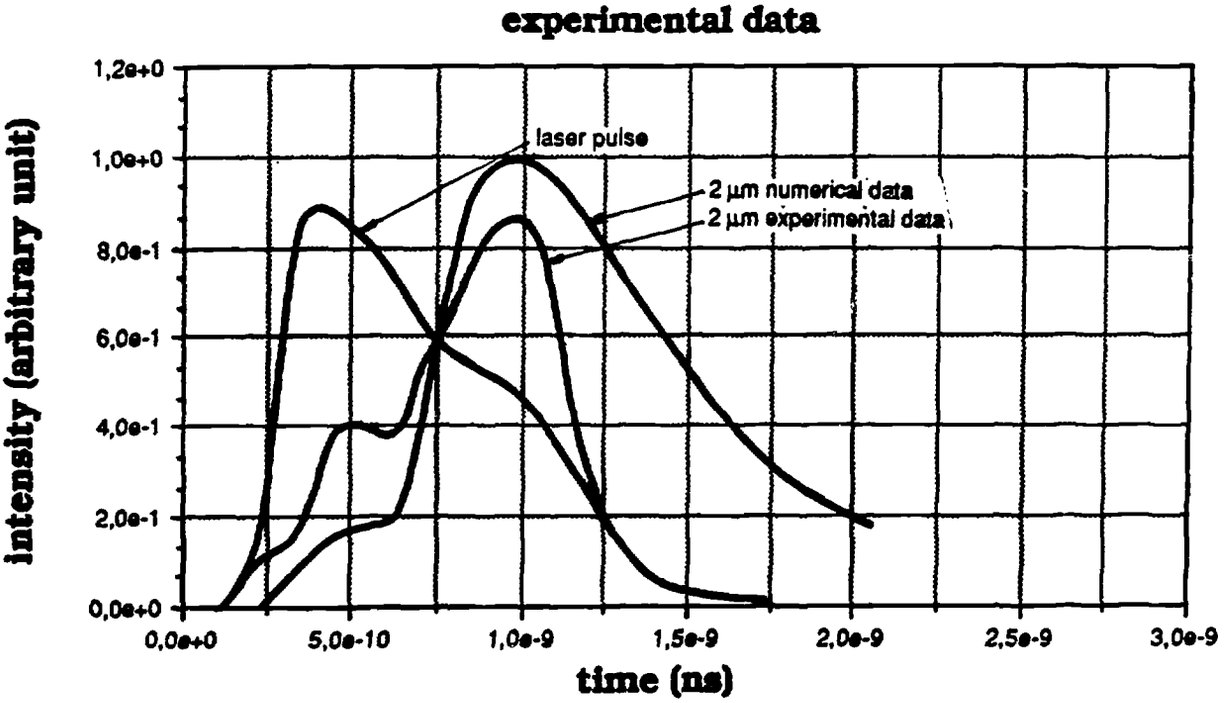
experimental data
intensity (arbitrary unit)
1,2e+0
1,0e+0
8,0e-1
6,0e-1
4,0e-1
2,0e-1
0,0e+0
laser pulse
2 µm numerical data
2 µm experimental data
0,0e+0
5,0e-10
1,0e-9
1,5e-9
2,0e-9
2,5e-9
3,0e-9
time (ns)

SPACE AND TIME EVOLUTION OF THIN GOLD FOIL

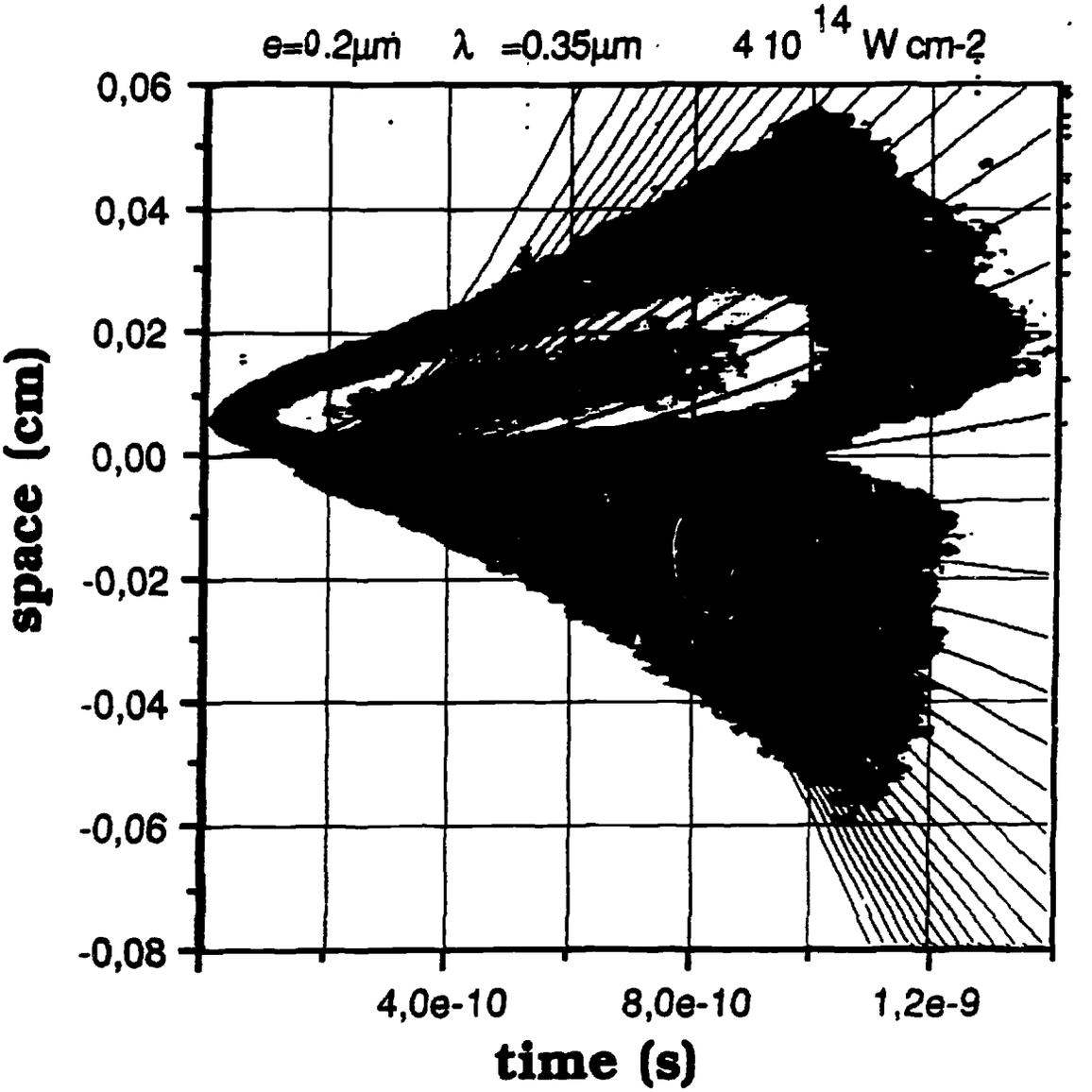

BEAM SMOOTHING EFFECT

- - BEAM NON UNIFORMITIES HAVE BEEN SMOOTHED OUT WITH AN OPTICAL FIBER OSCILLATOR ON P 102

  - WE USED ALSO R.P.P. ON OCTAL

- ABLATION DEPTH IN GOLD

  AT 1.06 µm : INSENSITIVE TO ANY SMOOTHING

  3 TIMES NUMERICAL SIMULATIONS

  FILAMENTATION ?

  AT 0.53 AND 0.35 µm: - REDUCED,

  - IN AGREEMENT WITH SIMULATIONS

- X-RAY CONVERSION

  NO SIGNIFICANT INCREASE
  LESS DISPERSION OF EXPERIMENTAL DATA
  REDUCTION OF HARD COMPONENT

b

X-RAY CONVERSION EFFICIENCY WITH AND WITHOUT OPTICAL SMOOTHING

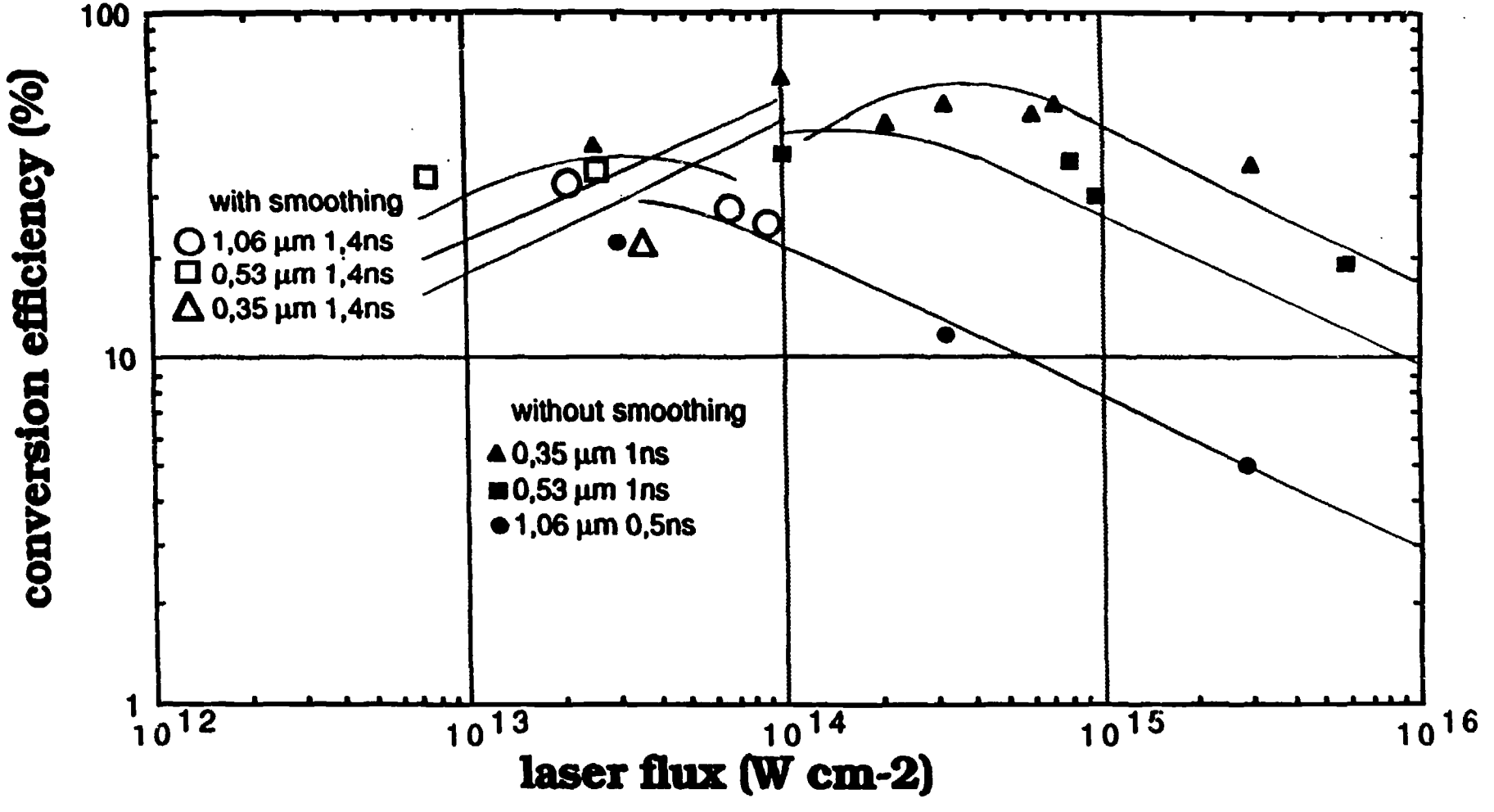

a

FRONT EMISSION LOBE OF GOLD TARGET WITH OPTICAL SMOOTHING

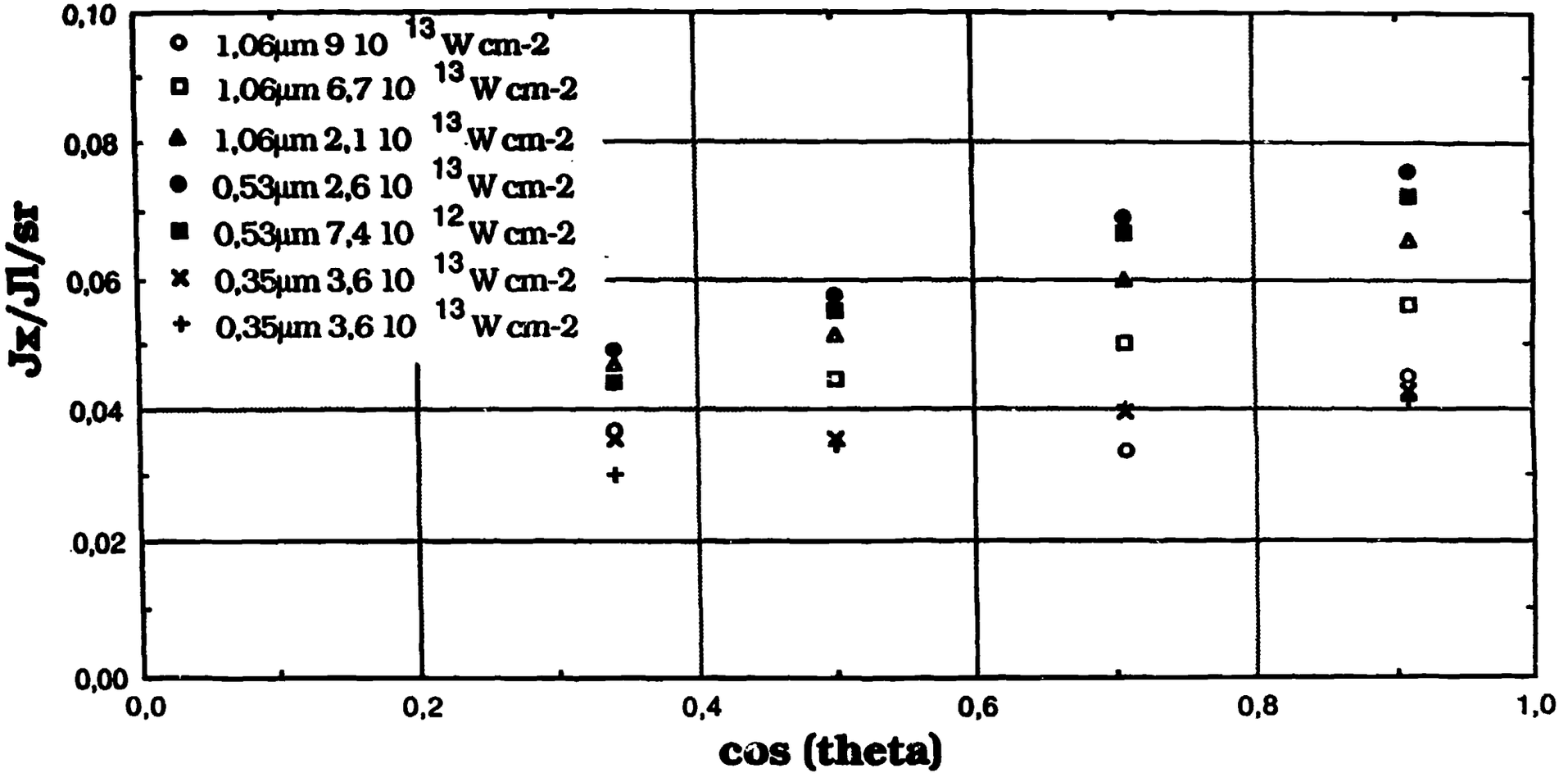

HARD X-RAY COMPONENT
WITH AND WITHOUT OPTICAL SMOOTHING

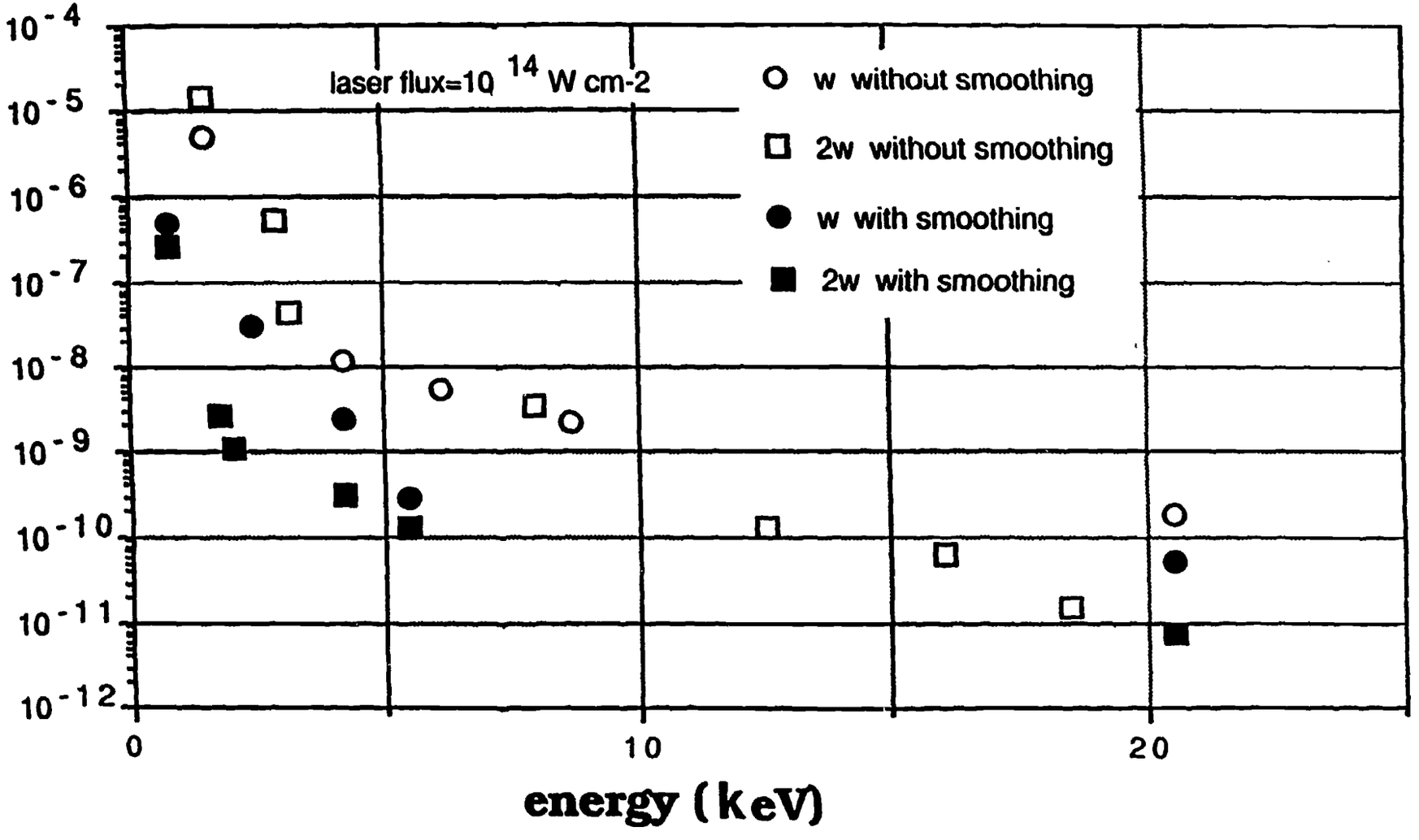

Exp OFO	Exp RPP	exp std	code
1.06µm 3.10^{13} W/cm^2 1ns			
110±10nm	110±10nm	110±10nm	30nm
0.53µm 10^{13} W/cm^2 1ns			
40±10nm			30-35nm *
0.35µm 10^{14} W/cm^2 1ns			
	200±10nm	450nm	200nm

HYDRODYNAMIC INSTABILITIES

- DEVELOPMENT OF A MIXING ZONE IN PLASMA SITUATION IS STUDIED USING LASER ACCELERATED TRI-LAYER PLANAR TARGETS

- TARGETS WITH ANTI-MIGRATION BARRIERS

- EXPERIMENTS ON OCTAL HAVE BEEN IMPROVED USING R.P.P.,

  $\lambda = 0.35\ \mu m$ $\qquad$ $\emptyset : 10^{13} - 5\ 10^{14}\ WCM^{-2}$

- TARGET HYDRODYNAMICAL BEHAVIOUR DETERMINED BY X-RAY SHADOW-GRAPHY

  EXP^{LE} $\qquad$ $\emptyset = 2.10^{14}\ WCM^{-2}$
  $V = 1.210^{7}\ CM\ S^{-1}$
  $\Gamma = 10^{16}\ CM\ S^{-2}$

- METHOD CHECKED BY COMPARISON WITH STABLE AU/AL/SI TARGETS (SMALL DENSITY JUMP BETWEEN AL AND SI)

Al LINE DUE TO THE MIXING Al/Au IN AN UNSTABLE TRILAYER

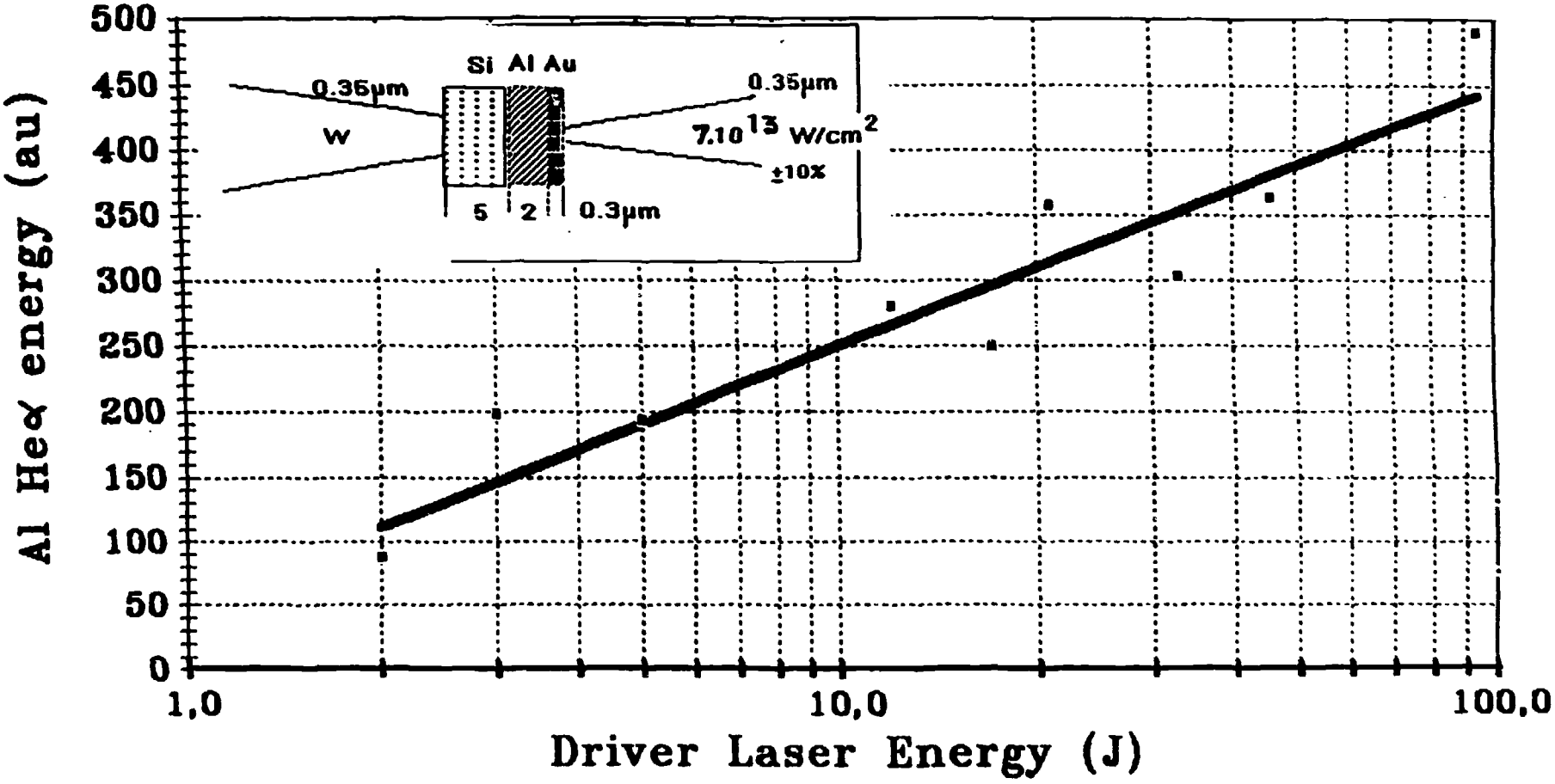

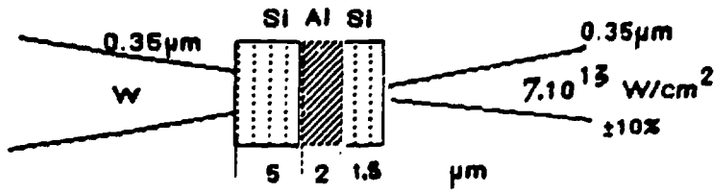

68J/27J SI(5) AL(2) SI(1.5H)

DELAY BETWEEN AL AND SI LINES
FOR A STABLE TRILAYER SI/AL/SI

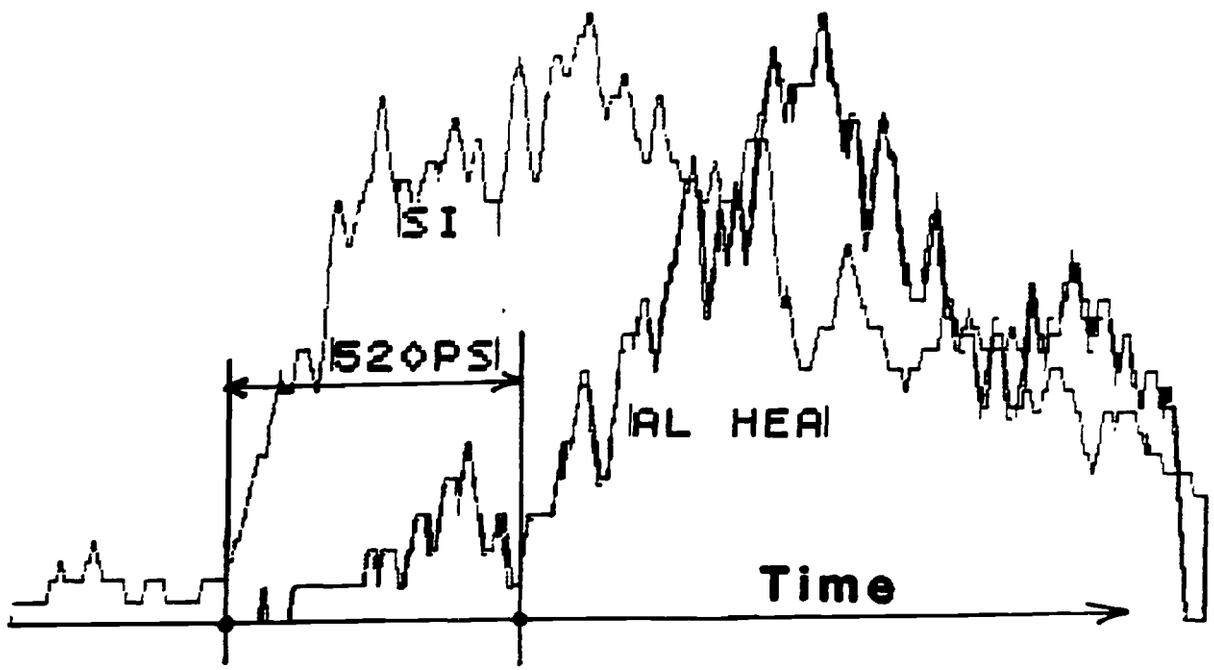

X-RAY DIAGNOSTICS

NUMEROUS DIAGNOSTICS ARE ROUTINELY OPERATED TO CHARACTERIZE THE PLASMA EMISSIONS IN THE X-UV AND SOFT X-RAY RANGE

RECENTLY DEVELOPED :

- F.M.S. STREAKED IMAGING SYSTEM 100 EV
  FLAT SIO2 GRAZING INCIDENCE MIRROR
  RESOLUTIONS 30 PS 8 LP MM^{-1}

- SPARTUVIX STREAKED SOFT X-RAY HIGH RESOLUTION SPECTROMETER
  TRANSMISSION GRATING
  RESOLUTIONS 30 PS 1 Å

- SMART STREAKED SOF X-RAY BROADBAND SPECTROMETER
  TRANSMISSION GRATING 40 EV - 1 KEV
  RESOLUTIONS 30 PS $10 < \frac{\lambda}{\Delta\lambda} < 100$

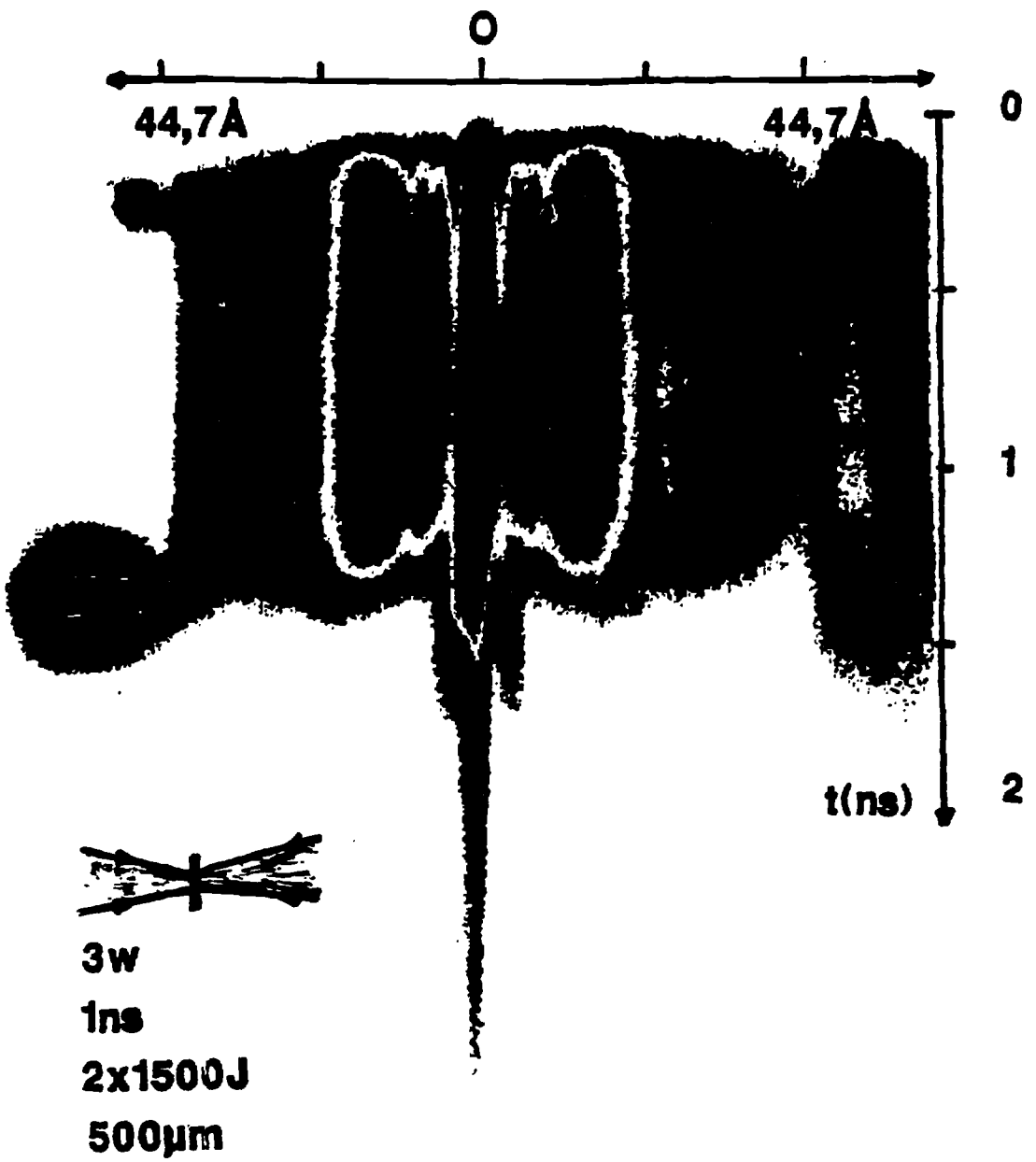
O
44,7Å
44,7Å
0
1
2
t(ns)
3w
1ns
2x1500J
500µm

NEUTRON DIAGNOSTICS

- FUEL $<\rho R>$ MEASUREMENT BY KNOCK-ON METHOD WITH CR 39.

$$<\rho R> = 5.4 \frac{N_K}{\Phi_N \Omega F} \text{ G.CM}^{-2}$$

WE HAVE DEVELOPED A COMPUTERIZED MICROSCOPE SYSTEM FOR AUTOMATED TREATMENT.

- PUSHER $<\rho \Delta R>$ MEASUREMENT BY RADIOCHEMISTRY MEASUREMENTS

  - AREAL DENSITY DEDUCED FROM SI^{28} ACTIVATION

  - FRACTION OF DEBRIS COLLECTION DEDUCED FROM N_A^{24} ACTIVITY

  - SENSITIVITY : $\Phi_N <\rho \Delta R> \geqslant 10^5$

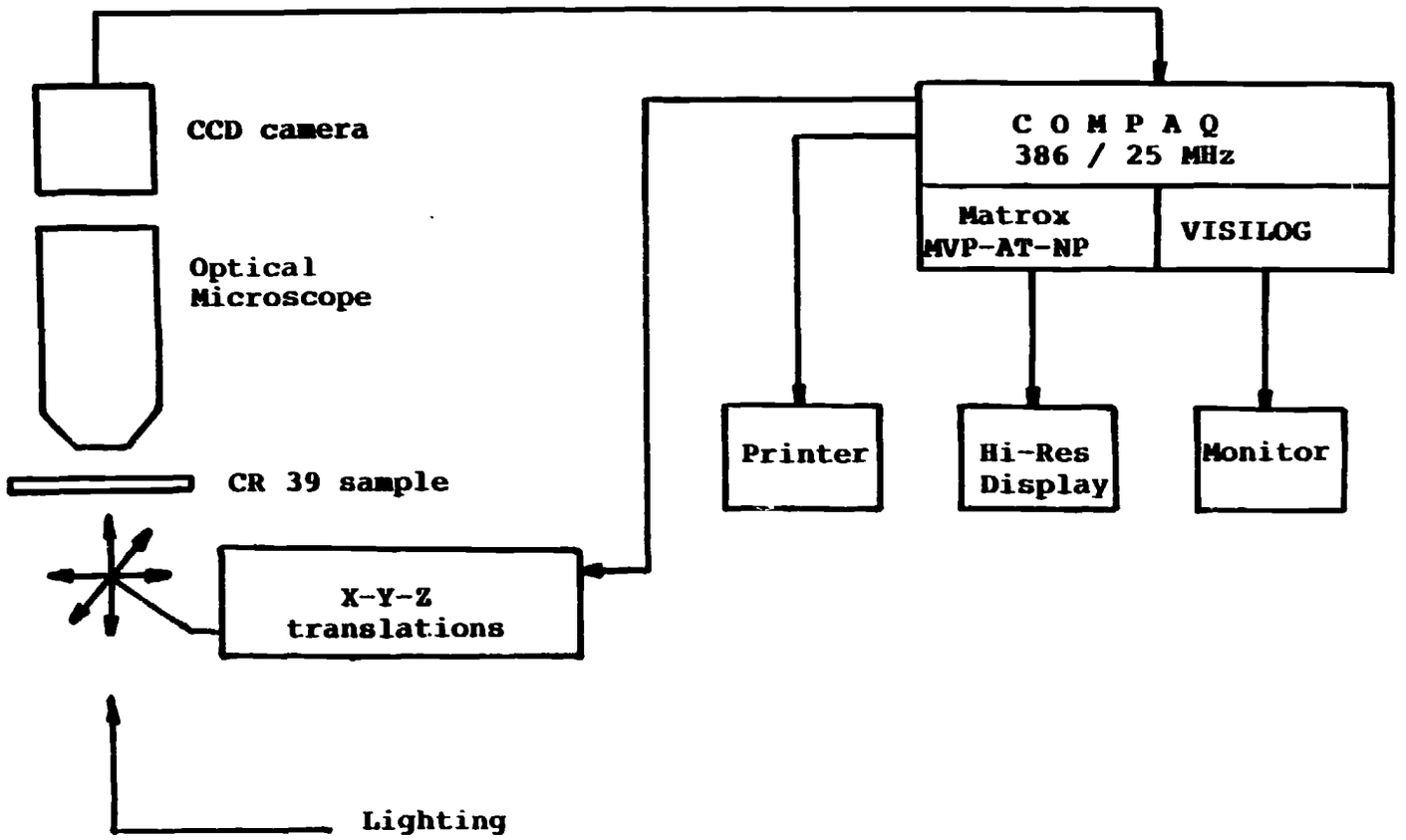

AUTOMATED TREATMENT OF KNOCK-ON RECORDING

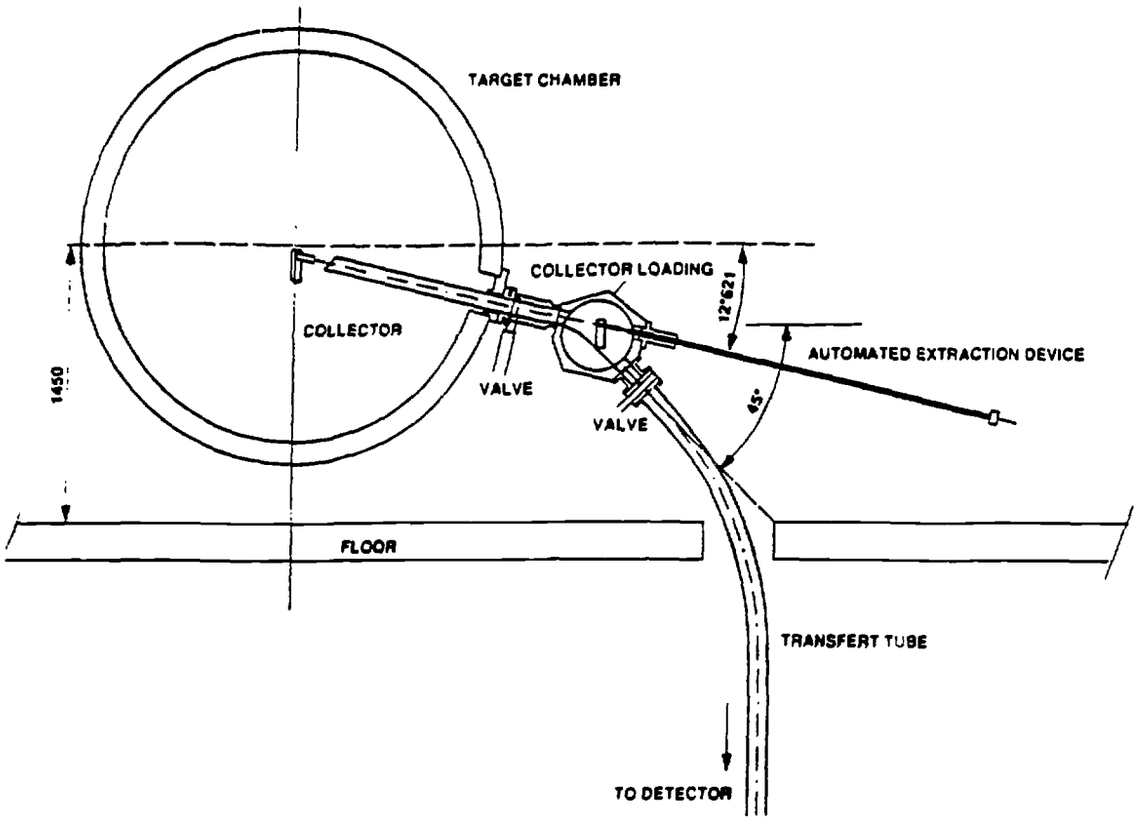

SCHEME OF THE FAST EXTRACTION TARGET DEBRIS COLLECTION SYSTEM FOR RADIOCHEMISTRY

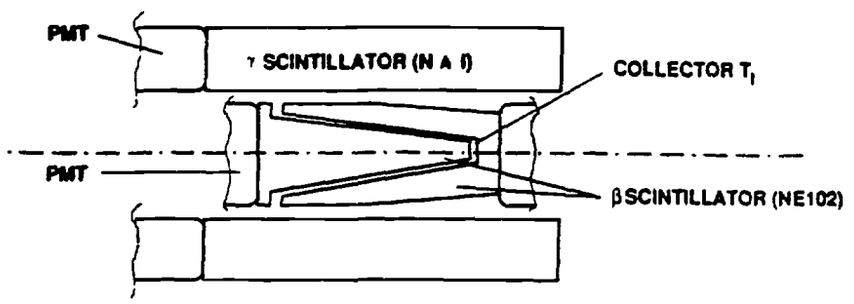

SCHEME OF THE 4π β γ DETECTOR

LASER RESEARCH : OPTICAL SMOOTHING

OPTICAL SMOOTHING BY OPTICAL FIBER OSCILLATOR HAS BEEN IMPLEMENTED ON P 102

- IMAGE OF THE FIBER OUTPUT RELAYED UP TO THE TARGET.

AT FUNDAMENTAL, RESIDUAL OSCILLATIONS $\leq$ 10%, AND SHARP EDGES.
THE SPECTRUM WIDTH IS CONSTANT OVER THE WHOLE LASER CHAIN.

AFTER FREQUENCY CONVERSION THE INITIAL SHAPE (EXP^{LE} : SQUARE SHAPE) VANISHES, AND THE SPECTRUM IS NARROWED.

- FREQUENCY CONVERSION WITH TYPE II KDP CRYSTALS EFFICIENCY :
  40% AT 2 WO ; 12% AT 3 WO

a

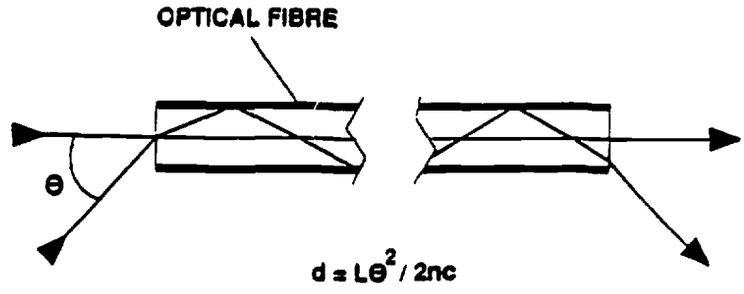

b

SPECTRAL BANDWIDTH IS STRONGLY REDUCED BY FREQUENCY CONVERSION

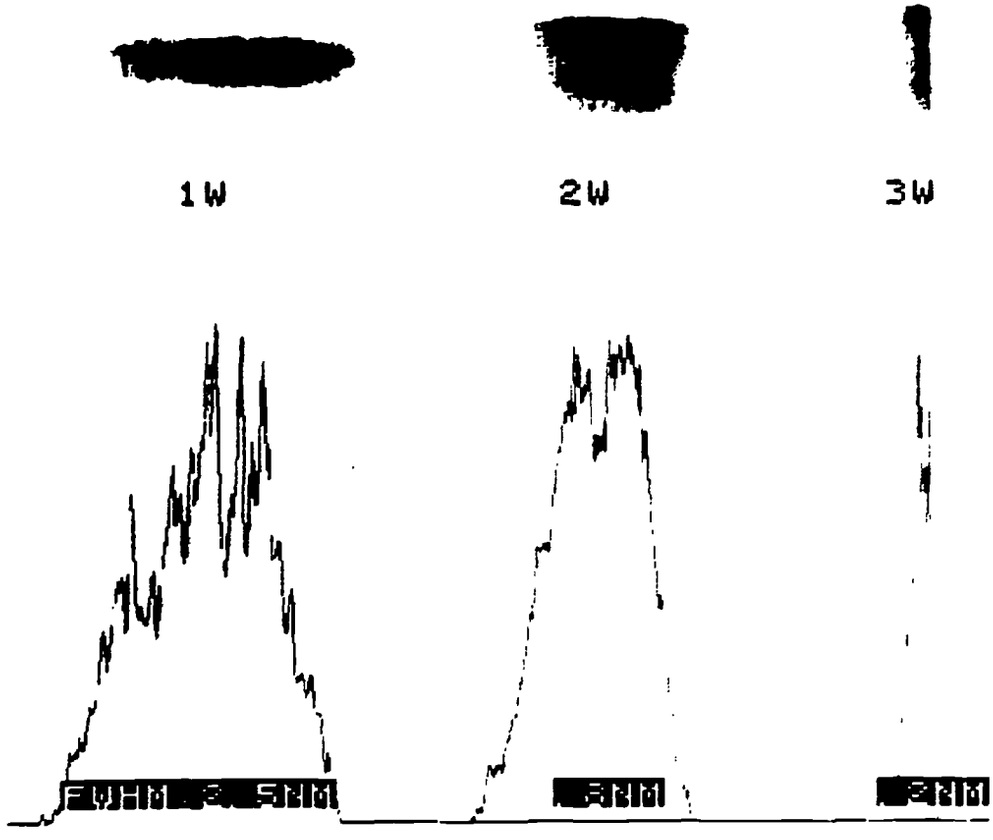

FOCAL SPOT PROFILES ARE MODIFIED BY FREQUENCY CONVERSION

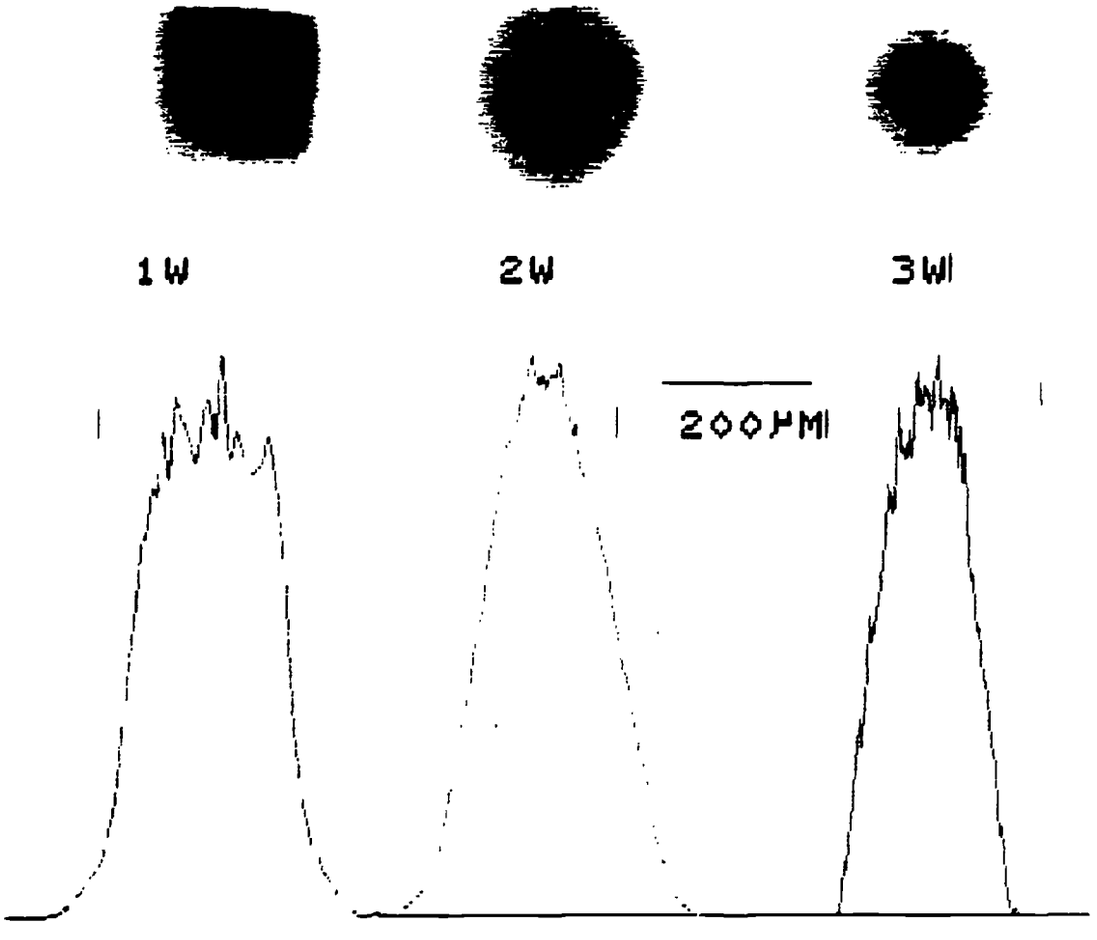

LASER RESEARCH : SOL GEL COATINGS

- EFFORT ON HIGH FLUENCES ANTIREFLEXION OR MIRROR COATINGS, IN SYNERGY WITH LLNL

- STARTING FROM COLLOIDAL SUSPENSIONS, HIGH-INDEX OPTICAL COATINGS HAVE BEEN PREPARED. AL_2O_3 ,H_2O APPEARED AS THE MORE DAMAGE RESISTANT

- HIGH REFLECTIVE COATINGS WERE PREPARED BY ALTERNATING HIGH INDEX COMPONENTS WITH $SI0_2$ COATINGS. THE AL_2O_3 - $SI0_2$ SYSTEM APPEARED TO BE THE STRONGEST

OXYDE	INDEX	DAMAGE AT 1064 nm.J/cm2		
		1ns, SINGLE SHOT	10ns, SINGLE SHOT	10ns, 30Hz
SiO2	1.20	14 - 15	30 - 40	30 - 40
Al2O3.H2O	1.43	11 - 14	30 - 40	40
ZrO2	1.48	7 - 10	10 - 20	10 - 15
HfO2	1.50	8 - 11	15 - 20	15 - 20
TiO2	1.80	8 - 10	15 - 20	2 - 5
ThO2	1.50	10 - 13	20 - 25	?

Damage thresholds of single-coatings

OXYDE-PAIR	DAMAGE AT 1064 nm.J/cm2		
	1ns, SINGLE SHOT	10ns, SINGLE SHOT	10ns, 30Hz
TiO2-SiO2	6 - 8	10	1 - 4
ZrO2-SiO2	6 - 7	10 - 15	10
HfO2-SiO2	5 - 8	15	15
ThO2-SiO2	8 - 9	20	?
Al2O3-SiO2	8 - 13	30 - 45	25 - 48

Damage thresholds of HR-coatings

CONCLUSION

- THE LASER PROGRAM AT CEL-V IS CONCENTRATED ON HIGH PERFORMANCES ABLATIVE IMPLOSION.

- INDIRECT DRIVE HAS BEEN CHOSEN AS THE MOST PROMISING APPROACH TOWARDS I.C.F.

  IMPROVEMENT OF IMPLOSION SPHERICITY HAS BEEN TESTED, IN CONJUNCTION WITH PROMISING RESULTS ON DOMINANT ISSUES SUCH AS RADIATIVE TRANSFER AND HYDRODYNAMIC INSTABILITIES.

- PROGRESS TOWARDS THIS END INCLUDES THE DEVELOPMENT OF NEW PLASMA DIAGNOSTICS, AND EFFORTS ON HIGH POWER LASER ADVANCED TECHNOLOGY